Investigating Altered Brain Metabolism in the TgF344-AD Rodent Model of Alzheimer's Disease Using in-vivo $_{13}$C Magnetic Resonance Spectroscopy

A thesis submitted to McGill University
in partial fulfillment of the requirements of the degree of
Master of Science

by

Steven Zhang
Integrated Program in Neuroscience
McGill University, Montreal

December 2019

Supervised by Jamie Near

Abstract

An estimated 30 million people worldwide suffer from Alzheimer's disease (AD), a neurodegenerative disorder characterized by memory loss and progressive cognitive impairment. Despite being the focus of enormous research efforts, there remains a lack of accurate pre-mortem diagnosis and effective treatments against AD. While major discoveries have uncovered some of the important pathophysiological processes underlying this disease, such as the aggregation of amyloid protein plaques and neurofibrillary tangles in the brain, AD continues to evade detection in its pre-symptomatic stages. One of the main hallmarks of AD pathology is a decrease in glucose metabolism that originates in the hippocampus and precuneus brain structures, and eventually spreads throughout the brain. Separately, there is increasing evidence that neuroinflammation plays a role in AD pathogenesis, however it remains unclear whether neuroinflammation and altered brain metabolism are linked.

Magnetic resonance spectroscopy (MRS) is a non-invasive imaging technique which can be used to study neurochemistry and brain metabolism in vivo. Specifically, Carbon-13 (^{13}C) MRS enables quantitative assessment of cerebral metabolism such as tricarboxylic acid (TCA) cycling and glutamate/glutamine neurotransmitter cycling rates. The aim of the current study is two-fold; 1) to investigate altered brain metabolism in a rat model of AD using ^{13}C MRS, and 2) to determine the effects, if any, of early treatment with the anti-inflammatory drug, Naproxen, on these metabolic changes.

Three rat cohorts, each containing ten rats, were investigated in the study; a wild type control cohort, a transgenic cohort with no treatment, and a transgenic cohort treated with

Naproxen from weaning up to 10 months of age. At 16-months of age, all three cohorts underwent ^{13}C MRS imaging during an infusion of [1,6-^{13}C] glucose. The rate of TCA cycle (V_{TCA}), the glutamate-alpha–ketoglutarate exchange rate (V_X), and the rate of neurotransmission (V_{NT}) were estimated by fitting the measured time courses of fractional ^{13}C enrichment to a metabolic model. Additionally, concentrations of seven metabolites (N-acetylaspartate, taurine, glutamate, myo-inositol, glutamine, glutathione, glycerophosphocholine (GPC), and phosphocholine (PCh)) were quantified, and concentrations of these metabolites were compared between groups.

Myo-Inositol levels were found to be elevated in both untreated and treated transgenic animals relative to wild type animals, suggesting an increase in neuroinflammation. Similarly, there was a significant increase in GPC+PCh concentrations in transgenic control animal relative to wild type animals, but no significant difference was observed between wild type and treated transgenic animals. This finding suggest that AD pathology is associated with elevated levels of both myo-Inositol and GPC-PCh, but that early treatment with anti-inflammatory drugs is only effective at reversing the elevations in GPC-PCh in a persistent way. ^{13}C MRS revealed no difference in metabolic flux rates between treated and untreated transgenic AD rats, but both groups exhibited significantly lower V_{TCA} and V_X fluxes relative to the wildtype group. The observation of decreased V_{TCA} in the AD cohorts is consistent with previous PET-based literature of hypometabolism and the confirmation of altered TCA cycle metabolism could serve as a potential biomarker for AD. Treatment with Naproxen did not rescue the impaired metabolism in AD rats, suggesting that the metabolic impairments observed in AD are not linked to neuroinflammation.

Résumé

Environ 30 millions de personnes dans le monde souffrent de la maladie d'Alzheimer (MA), une maladie neurodégénérative caractérisée par une perte de mémoire et une déficience cognitive progressive. Malgré les efforts considérables déployés en matière de recherche, le diagnostic pré-mortem précis et les traitements efficaces contre la MA font toujours défaut. Bien que des découvertes majeures aient mis au jour certains des processus physiopathologiques importants à l'origine de cette maladie, tels que l'agrégation de plaques de protéines amyloïdes et d'enchevêtrements neurofibrillaires dans le cerveau, la MA continue à échapper à la détection à ses stades pré-symptomatiques. L'une des principales caractéristiques de la pathologie de la MA est une diminution du métabolisme du glucose, qui prend naissance dans les structures cérébrales de l'hippocampe et du précunéus et se propage éventuellement dans tout le cerveau. Séparément, il est de plus en plus évident que la neuroinflammation joue un rôle dans la pathogenèse de la MA, mais les liens entre neuroinflammation et altération du métabolisme cérébral ne sont pas bien compris.

La spectroscopie à résonance magnétique (MRS) est une technique d'imagerie non invasive qui peut être utilisée pour étudier la neurochimie et le métabolisme cérébral in vivo. Spécifiquement, le carbone 13 (13C) MRS permet une évaluation quantitative plus poussée du métabolisme cérébral tel que le cycle de l'acide tricarboxylique (TCA) et les taux de cyclage des neurotransmetteurs glutamate / glutamine. Le but de la présente étude est double. 1) étudier le métabolisme cérébral altéré dans un modèle de MA de rat utilisant le MRC 13C chez le rat, et 2) déterminer les effets éventuels d'un traitement précoce par le naproxène, un médicament anti-inflammatoire, sur ces modifications métaboliques.

Trois cohortes de rats, contenant chacune dix rats, ont été étudiés dans l'étude; une cohorte de contrôle de type sauvage, une cohorte transgénique sans traitement et une cohorte transgénique traitée au Naproxen du sevrage jusqu'à l'âge de 10 mois. Les trois cohortes ont subi une imagerie MRS 13C au bout de 16 mois avec une perfusion de glucose [1,6-13C]. Le taux de cycle de TCA (VTCA), le taux d'échange de glutamate-alpha – cétoglutarate (VX) et le taux de neurotransmission (VNT) ont été estimés en ajustant l'évolution temporelle mesurée de l'enrichissement en 13C fractionnaire sur un modèle métabolique. En outre, les concentrations de sept métabolites (N-acétylaspartate, taurine, glutamate, myo-inositol, glutamine, glutathion, glycérophosphocholine (GPC) et phosphocholine (PCh)) ont été quantifiées et les concentrations de ces métabolites ont été comparées entre les groupes.

Les niveaux de myo-inositol étaient élevés chez les animaux transgéniques traités et non traités par rapport aux animaux normales, ce qui suggère une augmentation de la neuroinflammation. De même, il y avait une augmentation significative des concentrations de GPC + PCh chez l'animal témoin transgénique par rapport aux animaux de type sauvage, mais aucune différence significative n'a été observée entre les animaux transgéniques de type sauvage et traités. Le 13C MRS n'a révélé aucune différence dans les taux de flux métaboliques entre les rats AD transgéniques traités et non traités, mais les deux groupes présentaient des flux de VTCA et de VX nettement inférieurs à ceux du groupe de type sauvage. L'observation d'une diminution de la VTCA dans les cohortes de DA est conforme à la littérature antérieure sur l'hypométabolisme basée sur la PET et la confirmation de la modification du métabolisme du cycle du TCA pourrait servir de biomarqueur potentiel pour la MA. Le traitement au naproxène n'a pas permis de rétablir le métabolisme altéré chez les rats atteints de la MA, ce qui suggère que les altérations métaboliques observées dans la MA ne sont pas liées à la neuroinflammation.

Acknowledgements

First and foremost, I would like to say thank you to my supervisor, Jamie Near, who warmly introduced me to the fascinating field of magnetic resonance spectroscopy and patiently mentored me starting from the very basics. His continued guidance and support made this project possible while maintaining the delicate balance to fostering my academic independence. Thank you to my friends and colleagues in the Near lab who not only helped with my project but provided a pleasant and friendly atmosphere to work in. I owe thanks to my committee members, Pedro Rosa-Neto and Sylvia Villeneuve, for their suggestions and feedback.

On a personal note, I would like to thank my friends both here at home and internationally for their constant words of encouragement and late-night work sessions. Special thanks to Sean Zhang, Raina Fan, Jonathan Johnson, and Joyce Chan.

I am indebted to my animals; my hedgehog at home, Pam, whose company and constant affection kept me going and my rats at the lab, who made not only this project, but research in every scientific field possible.

Finally, I would like to thank my girlfriend Rachel, who despite being far away, always manages to be so close to my heart.

Contribution of Authors

Animal breeding was done by Caitlin Fowler[5]. Femoral artery and vein catherization surgeries were performed by Jim Gordon[3]. MRS coil and sequence were developed by Chathura Kuramagamage[4]. Data acquisition was performed by Masoumeh Dehghani[2] and Steven Zhang[1]. High resolution plasma MRS analysis was performed by the Drug Discovery Platform at the Research Institute of the McGill University Health Centre. All material appearing in this document including data processing, data analysis, statistics and figures were written by Steven Zhang[1].

1Integrated Program in Neuroscience,

2Department of Psychiatry, McGill University,

3Comparative Medicine and Animal Resources Centre, McGill University,

4Department of Radiology and Biomedical Imaging, Yale University,

5Department of Biomedical Engineering, McGill University

Chapter 1: Introduction and Literature Review

1.1 Alzheimer's Disease

1.1.1 Background

Dr. Alois Alzheimer first published his famous case study of Auguste Deter back in 1906. Ms. Deter was initially presented to the German Institution for the Mentally Ill with symptoms of impaired memory recall, loss of consciousness and motor function. After her death in 1906, post-mortem staining of her brain revealed what Alzheimer described as senile plaques and neurofibrillary tangles, which remain to be present-day hallmarks of Alzheimer's Disease. Alzheimer's disease (AD), is a neurodegenerative disorder and the leading cause of dementia in late adult life. The World Health Organization estimates that there are currently 50 million cases of dementia globally, of which 60%-70% are caused by AD pathology[1]. Due to continuous increases in life expectancy, the proportion of people older than 65, who are most at risk of developing AD, has increased from 7% to 12%; as a consequence, rates of AD are projected to double every 5 years[2]. An increase in prevalence will accordingly accelerate the socio-economic burden of AD on society, which is already substantial; In 2015, the cost of AD on the US economy was estimated to be $226 billion[3]. Clinically, AD is associated with early symptoms of short-term memory impairment, leading to deficits in other cognitive domains, such as language and motor functions with disease progression[4]. After initial presentation of symptoms, AD leads to the death of affected individual in anywhere from three to nine years[5].

AD can develop in two forms, sporadic and familial. Familial AD (FAD) is the hereditary form of AD caused from mutations of one of the three major genes: amyloid precursor protein (APP), Presenilin 1 (PSEN1) and Presenilin 2 (PSEN2). However, over 99% of cases of AD is

sporadic (SAD) without any familial link, and is hypothesized to develop due to a combination of environmental, and life style factors, with age being the single greatest risk factor[6].

Pathologically, AD is characterized by the formation of intracellular neurofibrillary tangles and extracellular amyloidal protein deposits contributing to senile plaques; however, these processes are not selective for cases of AD dementia alone. Despite over a century of research, there is a lack of both accurate pre-mortem diagnosis and effective treatment for AD. Currently available treatments such as acetylcholinesterase inhibitors aim to decelerate disease progression and minimize symptoms severity but have no etiological impact on the disease. The non-availability of effective treatment stems from a lack of knowledge on the mechanisms of how factors such as neurofibrillary tangles and plaques contribute to disease progression. A review of current literature shows a myriad of other pathways as potential processes that contribute to AD including genetics, oxidative stress, dysfunctional calcium homeostasis, hormonal, inflammatory-immunologic, and cell cycle dysregulation[7]. However, by far the most studied and central theory remains to be the amyloid cascade hypothesis along with the tau hyperphosphorylation as the major pathogenetic mechanisms.

1.1.2 Amyloid beta

Amyloid beta (Aβ) is a naturally occurring peptide in the human body that is derived from the proteolytic cleavage of amyloid precursor membrane protein (APP), expressed both in brain cells, and in peripheral organs. Aβ levels are known to be elevated in AD patients when compared to cognitively normal individuals[8]. There are two main forms of Aβ expressed after APP cleavage; Aβ42, the most aggregation-prone and neurotoxic form and Aβ40, which is nine times more

prominent than Aβ42 in the brain[9]. Under normal conditions, clearance of Aβ from the brain occurs through either phagocytosis or endocytosis by phagocytes and microglia. However, evidence from studies of cerebral spinal fluid suggests that the normal Aβ clearance pathways are disturbed in AD patients, thus providing a possible mechanism for pathological Aβ accumulation[10]. CSF levels of Aβ42 are significantly lowered in AD patients, reflecting its accumulation into plaques, neuronal damage and degeneration, and neocortical neurofibrillary pathology[10]. Additionally, APP and PSEN1/2 mutations, responsible for FAD, bias the cleavage of APP to lead to an increase in toxic Aβ42 species production compared to Aβ40. It is hypothesized that the increased ratio of Aβ42 to Aβ40 facilitates tau hyperphosphorylation, disrupts mitochondrial function, and dysregulates calcium homeostasis, resulting in synaptic failure, cognitive dysfunction and ultimately cell death[11-13]. The amyloid cascade hypothesis posits that amyloid plaques formed by aggregates of uncleared Aβ peptide are the primary feature of AD pathology. Pharmacological approaches aimed at reducing the cerebral Aβ load in AD mice have successfully decreased synaptic loss and the rescue of memory deficits in behavioral tasks, but these effects were not replicable in humans[14,15,16].

More recent work showed substantial evidence opposing amyloid accumulation being the central event in AD pathogenesis. Accumulation of Aβ naturally occurs with aging in both asymptomatic and symptomatic elderly patients, and is not correlated with cognitive decline or neuronal loss, preventing it from classifying disease pathology[17,18]. Positron emission tomography (PET) scans have repeatedly demonstrated many individuals who have significant amyloid plaque burden do not show symptoms of memory impairment[19]. While it remains to be seen whether Aβ

is the cause or a by-product of AD progression, there is no question that it plays a pivotal role in AD pathology.

1.1.3 Tau Pathology

Tau is a highly soluble microtubule-associated protein (MAP) that interacts with tubulin to stabilize microtubule assembly in the brain, facilitating synapse formation and neuronal growth. There are six different tau isoforms, each with own physiological role and are modified post-translationally via a multitude of mechanisms. Of these modifications, phosphorylation of tau has been well defined to play a role in AD pathology where all six tau isoforms are present in an often hyperphosphorylated state in intraneuronal aggregates known as neurofibrillary tangles (NFTs). The tau hypothesis of AD states that excessive or abnormal phosphorylation of tau results in the formation of NFTs which negatively regulates microtubule assembly. Furthermore, hyperphosphorylated tau disassembles existing microtubules by sequestering unphosphorylated tau and microtubule associated protein 1 and 2 (MAP1/2), leading to neurofibrillary degeneration and neuronal cell death. However, the interplay between tau pathology and the accumulation of amyloid is not understood. Several lines of evidence indicate that amyloid peptide causes initial tau hyper-phosphorylation and that the two proteins act synergistically to cause cell death[20]. In a 3xTg-AD mouse model containing human APP, PS1, and tau mutant transgenes, the appearance of Aβ precedes tau tangle formation, supporting tau pathology as a downstream event of amyloid pathology[21]. In the same study, removal of intraneuronal Aβ via immunotherapy led to the removal of early phosphorylated aggregates of tau[22]. Additionally, Aβ oligomers act in a self propagating fashion by inhibiting proteasome function resulting in further accumulation of Aβ and tau[23]. Hyperphosphorylation and aggregation of tau in neurons have also been demonstrated to cause

downstream secondary pathways involving inflammation, autophagy impairment, and impediment of axonal transport[24]. However, APP and APP/PS1 mice without tau mutation produce elevated levels of Aβ, without showing any evidence of tangle formation[25].

Interestingly, PET studies have found NFT accumulation to precede plaque deposition in human AD, contradicting the amyloid theory of tau phosphorylation[26]. In fact, tau pathology correlates much better than plaques with the clinical picture of neurodegeneration in AD[27,28]. It is evident that further research is required in the roles of these biomarkers, however a new direction considering their possible interactions and synergistic effects in AD should be considered.

1.1.4 Glucose Metabolism

Glucose is the primary energy source for the mammalian brain, which consumes around 25% of the body's glucose levels to produce adenosine tri-phosphate (ATP) for its normal physiological function[29]. Glucose consumption can therefore serve as an indicator of synaptic activity, the loss of which is one of the main features of AD. A reduction in glucose metabolism is a recognized hallmark of neurodegeneration and appears years before cognitive symptoms, making it an attractive potential biomarker for early detection of AD[30]. Cerebral metabolism of glucose typically takes place via aerobic cellular respiration through a series of steps consisting of glycolysis and the tricarboxylic acid (TCA) cycle (Fig 1). Briefly, glucose is transported through the blood brain barrier and undergoes glycolysis, converting it into pyruvate via a series of intermediate metabolites. Pyruvate then enters the mitochondria and undergoes oxidation by the enzyme pyruvate dehydrogenase, combining with coenzyme A to form acetyl coenzyme A (acetyl CoA). Acetyl CoA enters the TCA cycle, and is further metabolized to eventually produce 30-32 ATP molecules which are used to drive almost every energy-requiring reaction in the cell.

One of the metabolic intermediates in the TCA cycle, α-ketoglutarate (α-KG), can be converted via a reaction with glutamate dehydrogenase to form the predominant neurotransmitter glutamate. Glutamate is the major excitatory neurotransmitter, accounting for over 90% of all synaptic connections in the human brain. As such, disturbances of glutamate pathways in the nervous system are commonly observed in neurodegenerative disorders[31-33]. It is hypothesized in the case of AD, altered glutamate synaptic activity could stem from a decrease in de-novo glutamate synthesis from glucose as result of altered glucose metabolism. Indeed, PET studies using the fluorodeoxyglucose (FDG) tracer have found decreases in the rate of cerebral glucose metabolism in the hippocampus, and posterior cingulate to precuneus regions of the brain[34]. These results have been replicated in studies using standard ^{1}H MRS which showed increased concentrations of glucose and decreased concentrations of downstream metabolites such as glutamate and glutamine, suggesting lowered metabolism[35-37]. This pattern of hypometabolism is consistently found in the vast majority of clinically diagnosed AD patients, and in over 85% of pathologically confirmed AD cases[38]. Furthermore, unlike amyloid plaque loads, glucose hypometabolism in regions like the precuneus and posterior cingulate has been shown to correlate with cognitive impairment[39-41]. Longitudinal studies have also demonstrated that impaired glucose metabolism is a good predictor of disease progression from MCI to AD[42,43]. However, FDG-PET is limited in its ability to link these changes in neuronal energy production with their effects on downstream neurometabolic pathways such as the conversion from glucose to glutamate and glutamine. The [^{18}F] FDG glucose analog cannot be metabolized and remains trapped in tissue until after the radioactive ^{18}F label undergoes positron decay, after which the remaining FDG becomes glucose-6-phosphate with a heavy oxygen which is able to be metabolized[44]. Since metabolism occurs only after positron decay, the signal from PET imaging only reflects the uptake

of the [18F] FDG label and its phosphorylation by the hexokinase enzyme. As such, there is a need for another method to look at downstream processes in glucose metabolism to establish its role in AD pathology and potential as a biomarker.

1.1.5 Neuroinflammation

Separately, studies have shown evidence for early neuroinflammation in AD patients. It has been hypothesized that excessive inflammation is the link between Aβ aggregation and its downstream comorbidities, such as tau hyperphosphorylation, in AD[45]. Data from transgenic models indicate that activation of the complement system and cytokines occur as a result of Aβ aggregation and that many of these inflammatory mediators such as cyclin-dependent kinase 5 that are up-regulated by Aβ can serve to increase tau pathology[46,47]. Furthermore, these inflammatory responses produce reactive oxygen species, which damage cell membranes and lead to neurodegeneration[48,49]. Excessive activation of microglia is also a well-documented feature of AD pathology, whereby the macrophages secrete proinflammatory molecules in close proximity of amyloid beta plaques, resulting in neuroinflammation and neurodegeneration[50-52]. However, the link between neuroinflammation and altered brain metabolism, if any, is not well understood. One hypothesis is that early neuroinflammation contributes to neuronal damage, which gives rise to later metabolic impairments. As such, nonsteroidal anti-inflammatory drugs (NSAIDs) have been considered to have possible therapeutic value in treating symptoms of AD through cyclooxygenase (COX) inhibition[53]. COX genes are responsible for the synthesis of prostaglandins, which are lipid compounds responsible for vasodilation, inflammation, and anaphylaxis pathways. NSAIDs have been found to help mitigate amyloid deposition and tau hyperphosphorylation, reduce inflammation and improve cognitive performance in a triple transgenic AD mouse model[54]. The

therapeutic benefits of NSAIDs has become the target of clinical research in humans. Specifically, the NSAID Naproxen has gained traction over the years by showing potential to postpone or inhibit AD symptoms. Naproxen's mechanism of action revolves around non-selectively inhibiting both COX-1 and COX-2 genes thereby limiting the synthesis of prostaglandin and reducing inflammation[55]. The drug has undergone two AD prevention trials which show a possible benefit against cognitive decline if it was taken during the pre-symptomatic phase of the disease[56]. Further research is required to investigate the components of inflammation involved in AD pathology, and in determining appropriate therapeutic targets.

1.1.6 Rodent Models of AD

The development of genetically modified animal models of AD has greatly contributed to our overall understanding of the genome-associated pathologies of Alzheimer's. Most transgenic models of AD are mice due to the ease of genetic manipulation[57]. To date, a complete transgenic model that fully captures all aspects of AD has not been identified, however existing models can reliably reproduce specific hallmarks of AD which can be experimentally tested for potential therapeutic interventions. As the etiology of idiopathic AD is unknown, animal models have relied on using genetic mutations associated with FAD such as APP and PSEN1, with the rationale that downstream pathology of the initial genetic trigger are quite similar to SAD. Most transgenic mice with mutant APP develop pathology that is similar to that found in the human brain, including Aβ accumulation into extracellular plaques and elevated levels of Aβ42[58]. Furthermore, immunocytochemistry experiments have found that Aβ plaques found in the brains of AD transgenic mice are structurally similar to those found in the human brain[59]. Most AD transgenic models successfully replicate memory impairments, with cognitive deficits strongly correlative to

the appearance of extracellular plaques, further supporting the validity of animal models of AD[60]. Memory-based learning tasks such as the Morris water maze, fear conditioning or the radial arm water maze are typically used to test for cognitive acuity[61].

Despite these similarities, critics have questioned the translatability of rodent model results to humans due to two major factors. Firstly, these transgenic rodents have failed capture tau pathology, specifically the formation of NFTs, the other hallmark marker of human AD[62]. The mouse genome lacks the expression of a class of tau isoforms found in humans, and NFT formation could only be replicated by expressing additional mutated human tau genes. These multigenic AD transgenic models do develop NFTs similar to those seen in human brain, with Aβ pathology seeming to precede the onset of tau pathology, consistent with the amyloid cascade hypothesis[63]. The development of these models allowed for longitudinal investigations of the effects Aβ and tau has on behavioral measurements of cognitive decline. However, it is important to note that the employed tau mutations do not occur naturally in either the SAD or FAD forms of human AD, and therefore the development of tau-related toxicity in these rodent models could be argued to poorly reflect true AD pathology.

Secondly, as the models carry mutations found in FAD, it is obvious that they are not representative of late onset SAD, which affects more than 99% of AD patients. Despite sharing similar pathological features in the late stages of disease progression, FAD has an earlier disease onset, at around 40-50 years of age, and exhibit different disease pathologies compared to SAD[64]. Furthermore, transgenic mouse models fail to exhibit frank neuronal death which is present in FAD[65]. In addition, cognitive decline in these models is reversible by pharmacological reduction of Aβ which does not occur in humans. While transgenic models are a great tool to investigate the underpinning complexities of AD pathology, models that better encapsulate all aspects of the

disease needs to be developed to draw conclusions about therapeutic benefits. Recently, the transgenic TgF344-AD rat model of AD strain was developed by Cohen et al, which expresses all of the major hallmarks of human AD; Aβ plaque build-up, tau protein pathology, behavioral deficits, memory loss, and frank neuronal loss in the cerebral cortex and hippocampus[66]. This transgenic rat is created by expressing a Swedish mutated version of the human APP and the deletion of exon 9 in the human PSEN1 gene without additional insertion of mutated human tau gene, both increasing the production of oligomeric amyloid beta[67]. Neuronal loss as well as behavioral deficits are apparent by 16 months of age where memory related learning deficits in tasks such as the Morris water maze and Barnes maze were exhibited[68]. Rats in general exhibit far greater cognitive complexity compared to mice, making the TgF344-AD rat model promising for further AD research.

1.2 Magnetic Resonance Spectroscopy

1.2.1 Background

In vivo magnetic resonance spectroscopy (MRS) is a specialized non-invasive, radiation-free imaging technique that has been used to study metabolic changes in brain tumors, strokes, seizures, and other neurological diseases. It has also been used to study the metabolism of other organs such as muscles and tissues. Proton (^{1}H)-MRS is frequently used in a research setting in complement with the more common magnetic resonance imaging (MRI) technique. Both methods utilize the same underlying principles by typically acquire signal from hydrogen protons; MRI acquires signal primarily from protons which reside within water and fat whereas ^{1}H-MRS acquires the signal from protons attached to less concentrated molecules. MRS typically acquires its signal from a single localized region, referred to as a voxel, and allows for quantification of the relative

concentrations of a variety of metabolites. As MRS techniques suppress the large signals from water and fat, they can detect low millimolar concentration metabolites, making them ideal for studying cerebral metabolism. Different metabolites exhibit different NMR resonance frequencies based on their local chemical environments. These frequency differences are referred to as chemical shifts (δ) and are expressed in parts per million of the Larmor frequency, allowing for their identification. Once a localized NMR signal has been detected, a Fourier Transform (FT) of the signal decodes the frequency information contained in the time domain signal to reveal one or more spectral peaks corresponding to the metabolites in the selected voxel.

^{1}H MRS has been used extensively to study metabolic alterations in Alzheimer's disease in both humans and animal models. The specific metabolite changes observed include: increased myo-Inositol (Ins), reduced *N*-acetyl aspartate (NAA), reduced glutamate, and reduced glutamine. Elevated level of myo-Inositol is thought to be linked with heightened glial and microglial activity, reflecting increased neuroinflammation in AD pathology[69]. As NAA is observed in high concentration in neuronal tissue, its decrease is thought to represent neuronal or axonal loss[70].

1.2.2 Carbon-13 MRS

In order to study cerebral energy metabolism and neurotransmission in vivo, a technique known as ^{13}C spectroscopy can be used. Similar to how ^{1}H MRS looks at the signal from protons attached to other molecules, ^{13}C MRS looks at the signal generated from the ^{13}C isotope of carbon. Following the infusion of a ^{13}C labelled substrate, ^{13}C MRS is able to follow the substrate through its metabolic pathway and quantify the concentration of downstream intermediate metabolites, as well as the flux rates of the metabolic processes. Carbon-13 spectroscopy is less commonly performed due to its increased experimental complexity; ^{13}C has a low isotopic abundance of 1.1%,

resulting in a signal that is small and hard to detect when compared to ^{1}H MRS and requires dedicated hardware. However, the low natural abundance also makes ^{13}C MRS the ideal technique to investigate cerebral metabolism as there is virtually no background signal from naturally occurring ^{13}C. The process of ^{13}C MRS based metabolic studies can be divided into four steps; the infusion of the ^{13}C labelled substrate, the actual detection of the NMR signal, quantifying the spectral peaks and fractional enrichment of metabolites and finally metabolic modelling to estimate the metabolic fluxes. Recently, ^{13}C MRS has been used to study altered cerebral metabolism in the AβPP-PS1 mouse model of AD[71]. Ex-vivo NMR analysis was performed using brain tissue extracts and found reductions of neuronal glucose oxidation and neurotransmitter cycling fluxes of glutamatergic neurons in the cerebral cortex and hippocampus of AD mice.

1.2.3 Labeling Pathway

As glucose is the primary source of cerebral energy metabolism, it is the optimal substrate to infuse and has been used extensively in ^{13}C studies. The ^{13}C label typically replaces either the 1^{st} carbon position in [1-^{13}C]-glucose or both the 1^{st} and 6^{th} carbon in [1, 6-^{13}C]-glucose. The biochemistry of the labelled glucose remains the same allowing the ^{13}C signal to be followed through both glycolysis and the neuronal TCA cycle where the ^{13}C label is transferred onto the 4^{th} carbon of glutamate, [4-^{13}C]-glutamate on the first turn of the TCA cycle, and the 2^{nd} and 3^{rd} carbon [2-^{13}C]/[3-^{13}C]-glutamate on the second (Fig 1). As the conversion of glucose into pyruvate is symmetrical, the labelling pattern of downstream metabolites through glycolysis and TCA does not differ whether you use [1-^{13}C]-glucose or [1, 6-^{13}C]-glucose; however, the ^{13}C labeling will double with [1, 6-^{13}C]-glucose and therefore increase detection sensitivity.

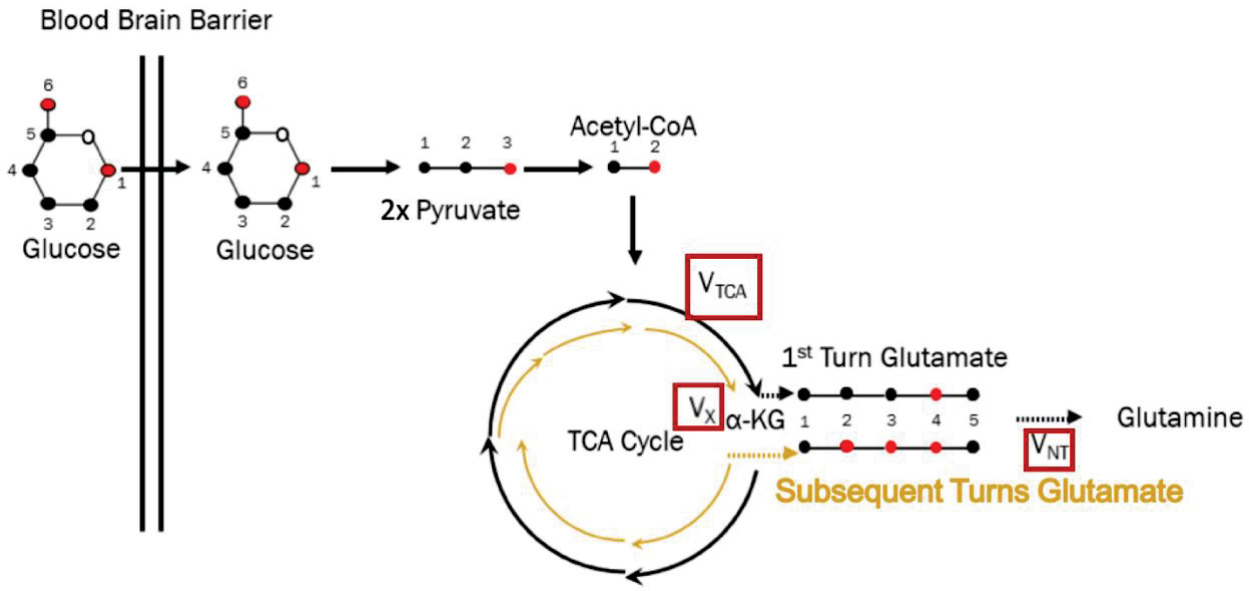

Figure 1: *Glucose Metabolism Pathway*
Overview of the steps of cerebral glucose metabolism as well as the conversion from glucose into glutamate and glutamine. Transfer of the ^{13}C label into intermediate metabolites is shown in red.
Abbreviations: TCA cycle, tricarboxylic acid cycle; α-KG, alpha ketoglutarate; V_X, flux of α-KG to glutamate; V_{TCA}, flux of TCA cycle; V_{NT}, flux of glutamate to glutamine.

1.2.4 NMR Detection

^{13}C NMR signals can be detected either directly, or indirectly through attached protons. Direct ^{13}C NMR detection provides increase spectral resolution as the chemical shift for ^{13}C extend over a wide range from 0 to over 200 ppm, allowing for close-by neighboring peaks to be easily resolvable even at lower magnetic field strengths. Multiple experiments have shown direct ^{13}C

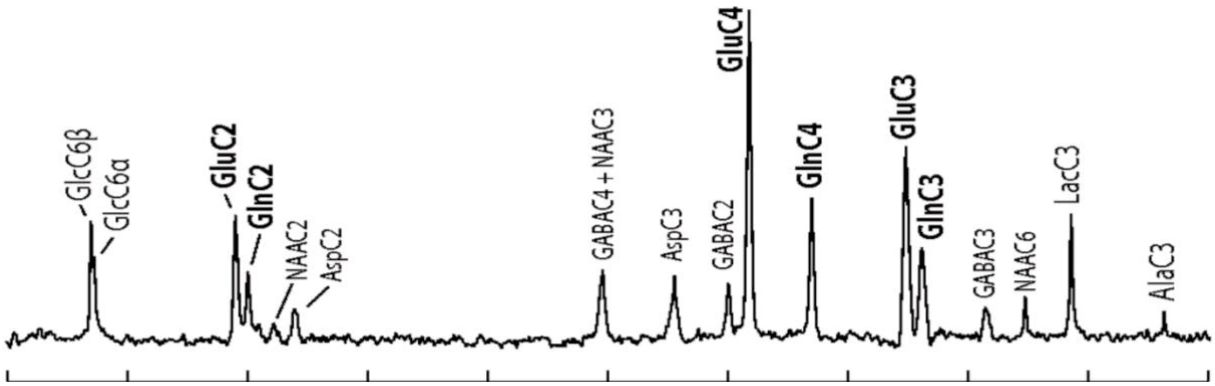

Figure 2: Direct ^{13}C MRS Spectra. Reprinted from *In vivo 13C MRS in the mouse brain at 14.1 Tesla and metabolic flux quantification under infusion of [1,6-$^{13}C_2$] glucose,* by Lai et Al, October 19, 2017.

MRS resolving glutamate and glutamine at C2, C3, and C4 positions, as well as aspartate and GABA at positions C2 and C3[72-74] as seen in Figure 2[75].

Indirect ^{1}H-[^{13}C] NMR detects instead the protons attached to the ^{13}C nuclei, whose signal can be isolated by virtue of heteronuclear J-coupling. Most indirect ^{1}H-[^{13}C] pulse-sequence incorporate heteronuclear J-difference editing to specifically select signals from ^{13}C coupled protons, combined with heteronuclear decoupling, which collapses the signal from the J-coupled satellite peaks, to detect the full ^{13}C-coupled proton signal at its original frequency[76]. This approach is sometimes called "proton-observed carbon-edited" spectroscopy, or POCE MRS outlined in Figure 3. Essentially, the sequence utilizes a specific echo time to take advantage of

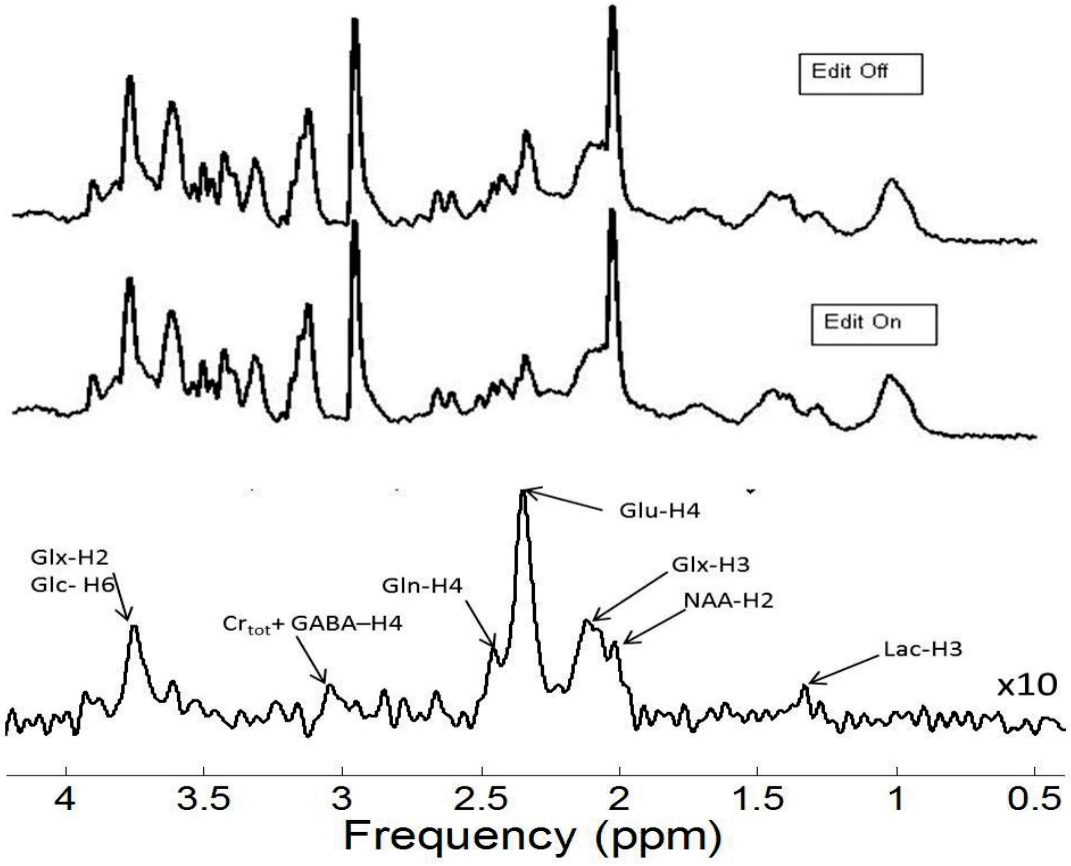

Figure 3: *^{1}H-[^{13}C] POCE MRS Spectra*
Spectra data from both the in phase ^{12}C+^{13}C signals (Edit Off) and out of phase ^{13}C signal (Edit On) are shown. Subtraction of these two scans result in a difference spectrum reflecting only the signal from ^{13}C coupled spins shown at the bottom.

the ^{13}C proton's scalar evolution phenomenon by producing two scans; one scan in which both coupled and uncoupled proton signals are in phase (Edit Off) and a second scan in which ^{13}C-coupled proton signals are exactly 180 degrees out of phase (Edit On). Subtraction of these two scans results in only the signal from protons experiencing a heteronuclear H-^{13}C coupling. The advantage of using indirect detection method is that proton has a larger gyromagnetic ratio approximately four times greater than ^{13}C, resulting in a higher precession frequency and significantly higher sensitivity at the same magnetic field strength. However, this comes at the cost of spectral resolution as even at higher fields of 7T, resolving glutamate and glutamine C3 continues to be problematic with indirect methods.

1.2.5 Peak Quantification

Spectral quantification is typically done using the LCModel software which fits the acquired spectrum to a linear combination of individual metabolite basis spectra in order to estimate the relative concentrations of each metabolite. Absolute quantification of metabolite concentrations can then be achieved by comparing each metabolite's signal intensity against that of an internal reference such as water or creatine, the concentrations of which are approximately known or can be assumed. The quantification of ^{13}C label incorporated into metabolites can be expressed as a fractional enrichment (FE) which is defined as the concentration of label ^{13}C in the metabolite divided by the summed concentrations of ^{13}C and ^{12}C in the metabolite. The time courses of [4-^{13}C]-glutamate and [4-^{13}C]-glutamine FE following ^{13}C labelled substrate infusion can then be calculated by dividing the amount of labelled signal by its original pre-infusion value at each time point. The fractional enrichment of these metabolites can then be used in metabolic modelling to calculate the rate of labeling as a measurement of metabolic flux.

1.2.6 Metabolic Modelling

To quantitatively measure the fluxes of these metabolic pathways, a mathematical model of the underlying labeling processes must be developed to fit the measured fractional enrichments. Most metabolic models of cerebral glucose metabolism assume that all influxes into the system equals to its effluxes and that the size of metabolic pools remain constant[77]. A series of differential equations can then be written to describe the transfer of the ^{13}C label from glucose to the detected metabolites namely glutamate and glutamine[78]. The number of equations written, and which specific pathways are tracked is determined by the model adopted to best reflect what is being experimentally measured. Two primary models are used in literature for *in vivo* ^{13}C NMR; a single-compartment model that examines the metabolic pathway of ^{13}C label transfer from glucose to C4 and C3 glutamate occurring in neurons (Fig 1), and a more complex two-compartment model that incorporates both neuronal and astrocyte contributions to glucose metabolism[73]. As the TCA cycle is believed to be a predominantly neuronal process, the one compartment model can robustly measure TCA cycle flux (V_{TCA}) and the rate of transfer from alpha ketoglutarate to glutamate (V_X) by inputting the measured [3-^{13}C]- and [4-^{13}C]-glutamate concentrations[79]. The exchange from the labelled glutamate pool to glutamine pool (V_{NT}) is then modelled using the measured time courses for labelled C3, C4 glutamate and C3 and C4 glutamine as well. The two-compartment model differs by considering the neuron and astrocyte as separate compartments, in order to have a greater overview of the entirety of the downstream metabolic pathways, especially the labeling of the glutamine pool which is thought to occur predominantly in astrocytes[80]. This model typically requires the addition of a complete glial compartment with its own TCA cycle as well as multiple other flux equations. While this model provides a more complete picture of the breakdown of glucose, it is much more complex and relies on assumptions for the respective contributions of

neuronal and glial cells to each cycle's flux. As the number of free parameters increases with the glial component, the robustness of the model is more dependent on the amount of experimental data needed, such as labelling of C3 and even C2 carbons of glutamate and glutamine which requires either a direct ^{13}C approach, or extremely high fields[81]. Two compartment model ^{13}C MRS experiments may also be employed following the infusion of ^{13}C labelled [2-^{13}C]acetate or [1, 2-^{13}C] acetate which is known to be mainly metabolized in astrocytes in order to quantify both neuronal and astrocyte compartments[82,83]. In both cases, the robustness of the model should be tested with Monte-Carlo simulations where noise is introduced at random to the measured fractional enrichment values through hundreds of iterations to estimate the standard deviation and degree of confidence for the estimated fluxes. Regardless of which model is used, an input function for the substrate entry in the brain is required. This is typically done by collecting samples of arterial blood to determine the concentration of ^{13}C labelling in the plasma followed by modelling using reversible Michaelis-Menten equations to estimate the amount transported through the blood brain barrier[84,85]. ^{13}C MRS studies using both models have shown that it is feasible to study cerebral metabolic fluxes in rodents, primates, and humans and the technique is starting to be implemented to research neurotransmission disease pathologies[86-90].

Chapter 2: The Current Study

2.1 Rationale for Study

The overall rationale of this project is to investigate altered brain metabolism in a rodent model of AD. As mentioned above, previous studies using FDG-PET, have found lower glucose uptake in AD patients compared to healthy controls, suggesting lower total glucose metabolism. However, the specific downstream metabolic alterations remain poorly understood. In this study, we will use ^{13}C MRS to investigate alterations in specific downstream glucose metabolism pathways in a rodent model of AD. This work will contribute significantly to the field of AD research by developing non-invasive imaging tools for assessment of disease status, and evaluation of therapeutic efficacy in animal models; discoveries which will ultimately be translatable to human AD patients.

2.2 Specific Aims and Hypotheses

The first specific aim of this study is to perform ^{1}H MRS to investigate differences in metabolite concentrations between wild type and the TgF344-AD transgenic rats. Based on previously published ^{1}H-MRS studies in AD rodent models, I hypothesize that the transgenic rats will exhibit elevated Ins levels and lowered NAA concentrations compared to wild type animals.

The second specific aim of the study is to apply indirect ^{1}H-[^{13}C] MRS to detect alterations in energy metabolism and neurotransmitter cycling rates in the TgF344-AD rat model of AD. I hypothesize that TgF344-AD rats will exhibit reduced TCA cycle and glutamate/glutamine neurotransmitter cycling rates relative to wild type rats.

The third specific aim of this study is to investigate the effects of pre-symptomatic Naproxen treatment on metabolic changes in the same rat model of AD. *In vivo* ^{13}C MRS studies of Naproxen treated subjects could lead to a deeper understanding linking effects of neuroinflammation and the neuronal metabolic alterations present in AD pathology. Therefore, we aimed to test the effects of neuroinflammation by studying brain metabolism in AD rodents with and without anti-inflammatory treatment. If metabolic impairments are caused by early neuroinflammation, then we would expect rodents treated with Naproxen to have less metabolic impairment compared with untreated rats. I hypothesize that early treatment of Naproxen on this rat model of AD will protect them from reductions in both TCA Cycle flux rates, as well as glutamate glutamine neurotransmission rates.

The experimental study design is shown below in Figure 4. After weaning, the transgenic treated cohort underwent Naproxen treatment until 10 months of age to test for presymptomatic treatment benefits. Significant AD pathologies expressed in the transgenic rats are listed at the 6, 15, and 16-month time points. All three rat cohorts underwent ^{13}C MRS scans at 16 months of age.

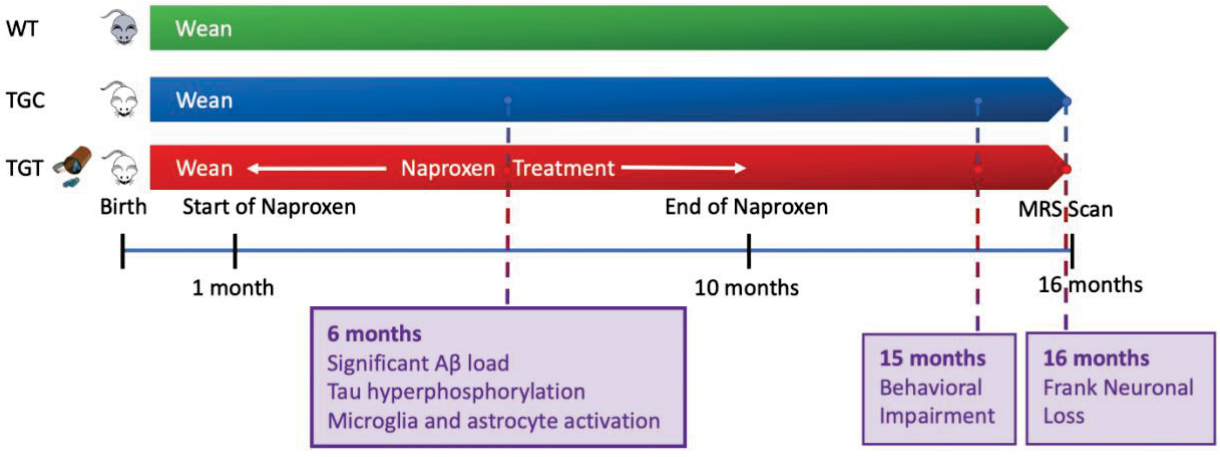

Figure 4: *Study Design*
Timeline of the three rat cohorts in the study is shown. Pathological timepoints are obtained from the TgF344-AD rat model described in section 1.1.6 Rodent Models of AD.

Chapter 3: Methodology

3.1 Animal Preparation

Three different cohorts (wild type, untreated transgenic, and Naproxen treated transgenic) with ten rats per group were used for the experimental design of this study. Wild type rats were bred from Fischer 344 (F334/NHsd) male and females. To obtain transgenic rats, hemizygous male TgF344-AD rats on a Fischer 344 background were bred with homozygous F344/NHsd wildtype females. The offspring of these breeding pairs were genotyped by collecting tail samples, and only the hemizygous transgenic offspring were studied. The TgF344-AD model is a double transgenic line that expresses both the "Swedish" mutant human APP (APPswe; APP KM670/671NL) and deletion of exon 9 mutant human presenilin-1 (PS1ΔE9). For the transgenic strain, rats were split into a transgenic treatment group to receive Naproxen and a transgenic control to receive no treatment. Beginning at one week of age, rats in the treatment group were administered Naproxen orally through their chow, which was formulated with a concentration of 375 ppm. Naproxen treatment continued until 10 months of age, at which point it was stopped. ^{13}C MRS scans for all three cohorts took place at 16 months of age, when TgF344-AD rats exhibit amyloid and tau pathologies and behavioural deficits are fully developed. Typically, female rats weighed between 200-300g and male rats weighed 500-600g by the time of scanning, and all rats were housed two per cage. Animal preparation and procedures were previously approved by McGill University's animal research committee and are in accordance with guidelines set by the Council on Animal Care.

3.2 Surgical Procedure and Infusion

On the day of the ^{13}C MRS scan, following an overnight fast of 15 hours, the femoral artery and vein of the rat were cannulated under free-breathing of 2% isoflurane anesthesia using 30 cm 1.9 to 3 Fr catheters from (Instech Laboratories, Plymout Meeting, PA, USA). The thin diameter of the catheter is necessary for arterial insertion, especially for female rats, and the length of the catheter needs to adequately extend out from the scanner bore to allow for blood draw. This procedure guarantees the infusion of [1,6-^{13}C] glucose directly into the blood stream through the femoral vein. The same incision allows for the cannulation of the femoral artery for sampling of glucose concentrations in the plasma, which is needed for metabolic modelling. Special care was required regarding the cannulation procedure due to the difficulty of the procedure. Firstly, the femoral artery and veins are extremely thin and delicate vessels which may easily rupture during the procedure even with an experienced veterinarian, however the same vessels on the contralateral side were used in case of vessel tearing. Alternative methods such as a tail vein cannulation or jugular cannulation could be used as a last resort but would not be ideal due to the difficulty of reliably cannulating the tail vein, and the jugular incision site being in close proximity to the surface head coil, which may affect animal positioning and image quality. Post-surgery, the animal was maintained under anesthesia and head-first prone positioned in the MRI scanner with a ^{1}H-[^{13}C] coil setup previously developed in our lab[36]. [1,6-^{13}C]glucose (1.4 M, 20g/100mL), chosen as the ^{13}C signal yield is doubled as compared to single labeled glucose, was prepared in saline and infused intravenously through the femoral vein using a Harvard Apparatus PHD2000 infusion pump following the first baseline MRS scan. The infusion protocol consists of an initial bolus infusion over 15 seconds, which is then tapered off exponentially every 30 seconds in a step-wise fashion designed to rapidly raise and maintain plasma glucose levels at ~20mM with a 70%

fractional enrichment as seen in previous literature[91]. An average of 2.5 mL glucose solution was usually infused per female rats and 6 mL for males. Throughout the scanning session, the animal was heated with 32°C air in the magnetic bore, and the level of anesthesia was adjusted to maintain a respiration rate of roughly 40 breaths per minute.

3.3 MRS Set-Up

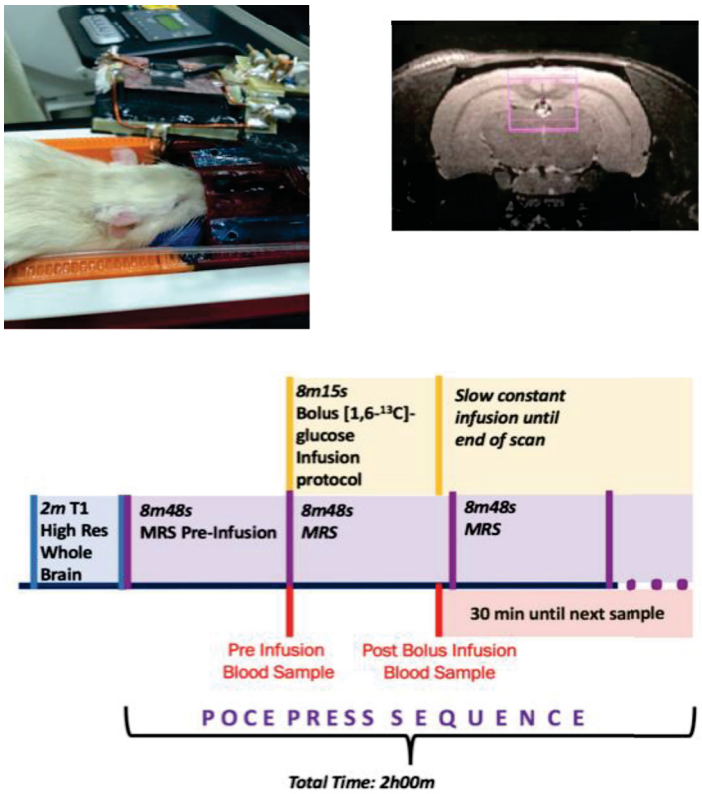

Figure 5 *Set-up for in vivo 13C MRS*
Home made 1H/13C surface coil and animal head placement is shown. Voxel is selected in the hippocampal region prior to scanning. Time line of scan overview is shown: a T1-weighted high-resolution structural scan is first performed for voxel selection, followed by a baseline MRS scan and pre-infusion blood sample. Infusion begins partnered with repeated MRS scans for the two-hour period with periodic blood sampling every thirty minutes.

Details of the MRS timeline as well as animal preparation are briefly shown in Figure 5. Indirect 1H-[13C] MRS scans were performed on a 7T Bruker Biospec 70/30 horizontal bore preclinical scanner with an actively shielded gradient insert (120 mm inner diameter, 650 mT/m in 150 µs). (Bruker, Massachusetts, USA). As previously mentioned, the indirect POCE detection

method yields a higher sensitivity in detecting the ^{13}C signal compared with direct ^{13}C methods, enabling us to achieve better spatial resolution, and to better quantify the label transfer into downstream glucose metabolites. All MR data were acquired with a custom built ^{1}H-[^{13}C] coil[92]. The ^{1}H-[^{13}C] surface coil is paired with an 86-mm volumetric resonator for homogeneous B_1 transmission. The ^{1}H-[^{13}C] surface coil consists of a ^{1}H receive (Rx)-only surface coil and a quadrature driven ^{13}C transmit (Tx) surface coil (for heteronuclear decoupling and editing pulses). The ^{1}H Rx-only surface coil provides sensitivity gains compared with a volume coil approach; the requirement for a T/R switch (and related losses) before the ^{1}H preamplifier is avoided. Furthermore, a high-pass filter and preamplifier can be placed proximal to the coil, further minimizing SNR losses inherent with POCE-MRS systems described in the literature. Prior to each scan, the ^{1}H Rx-only surface coil was tuned and matched to 300.3 MHz, and quadrature ^{13}C loops were tuned and matched to 75.5 MHz using a Morris RF Sweeper (Morris Instruments Inc., Ottawa, Canada). A high resolution T1-weighted structural image was first taken using the RARE sequence (TR/TE = 2713/10.8 ms, acquisition time = 2-minutes) to guide selection of a 100 μL volume of interest (4 x 5 x 5 mm^3 voxel) in the hippocampus and posterior cingulate region (Fig 5). These cortical structures were chosen as they are known to be among the first affected nuclei in AD pathology, and glucose metabolism and neurotransmission deficits in these areas are believed to underlie early memory impairments[93-95]. Localized water-suppressed ^{1}H spectra were acquired using a PRESS-based POCE PRESS sequence with simultaneous editing and localization pulses (SEAL-PRESS), TR/TE = 4000/8.13 ms, 6000 Hz spectral width, 128 averages, with an 8 min 48s acquisition time[76]. This sequence has a short echo time of 8.1 ms compared to 12.6ms for a typical PRESS-based POCE sequence, increasing the sensitivity for 4-^{13}C and 3-^{13}C labelled glutamate and glutamine by more than 20%. First- and second-order B_0 shimming was performed

using FASTMAP until a water line width of ~10Hz was achieved and VAPOR was used for water suppression using Gaussian pulses (length = 27 ms and 17.1 ms, bandwidth = 200 Hz)[96]. WALTZ-16 was used for heteronuclear decoupling during the first 200 ms of the acquisition[97]. The WALTZ composite pulse segment was empirically determined in phantoms to be 0.7 ms in length to provide >70% decoupling efficiency in the 20–60 ppm ^{13}C spectral bandwidth on a $6 \times 6 \times 6$ mm^3 voxel. One baseline scan was performed to establish baseline metabolic concentrations prior to infusion of [1, 6-^{13}C] glucose, followed by 15 sequential acquisitions during and following the infusion. The total scan time, including animal set up in the MRI, was typically two hours.

3.4 Plasma Collection and Processing

Arterial blood samples were taken prior to and immediately after glucose infusion through the femoral artery, and regular arterial blood samples were taken every thirty minutes thereafter. A OneTouch Ultra 2 glucose meter (LifeScan, Canada) was used to verify glucose levels after infusion but was inconsistent in measuring precise plasma glucose concentration. As such, arterial blood samples were centrifuged at 2000 rpm for ten minutes before extracting the plasma and storing in a -80°C freezer.

Plasma samples were later analyzed using a high resolution 400 MHz Bruker Ascend NMR spectrometer, and processed using Bruker TopSpin (Bruker, USA) for glucose concentration quantification and ^{13}C label fractional enrichment to be used as input functions for metabolic modelling (Fig 6). Samples were first thawed slowly to room temperature, ensuring to not damage the plasma proteins. Following which they were centrifuged at 4°C and 18000 RPM for 15 minutes to ensure plasma separation. 110 uL of plasma was then aliquoted using a pipette into individual

Eppendorf tubes and centrifuged again for 5 minutes at the same speed and temperature. Plasma samples would then be processed by a Gilson Liquid Sampler, adding a phosphate buffer to the solution for NMR. A tetramethylsilane reference was used as the internal standard for chemical shift calibration and spectral reference at 0 ppm. As well, a 5nM benzoic acid sample was used as

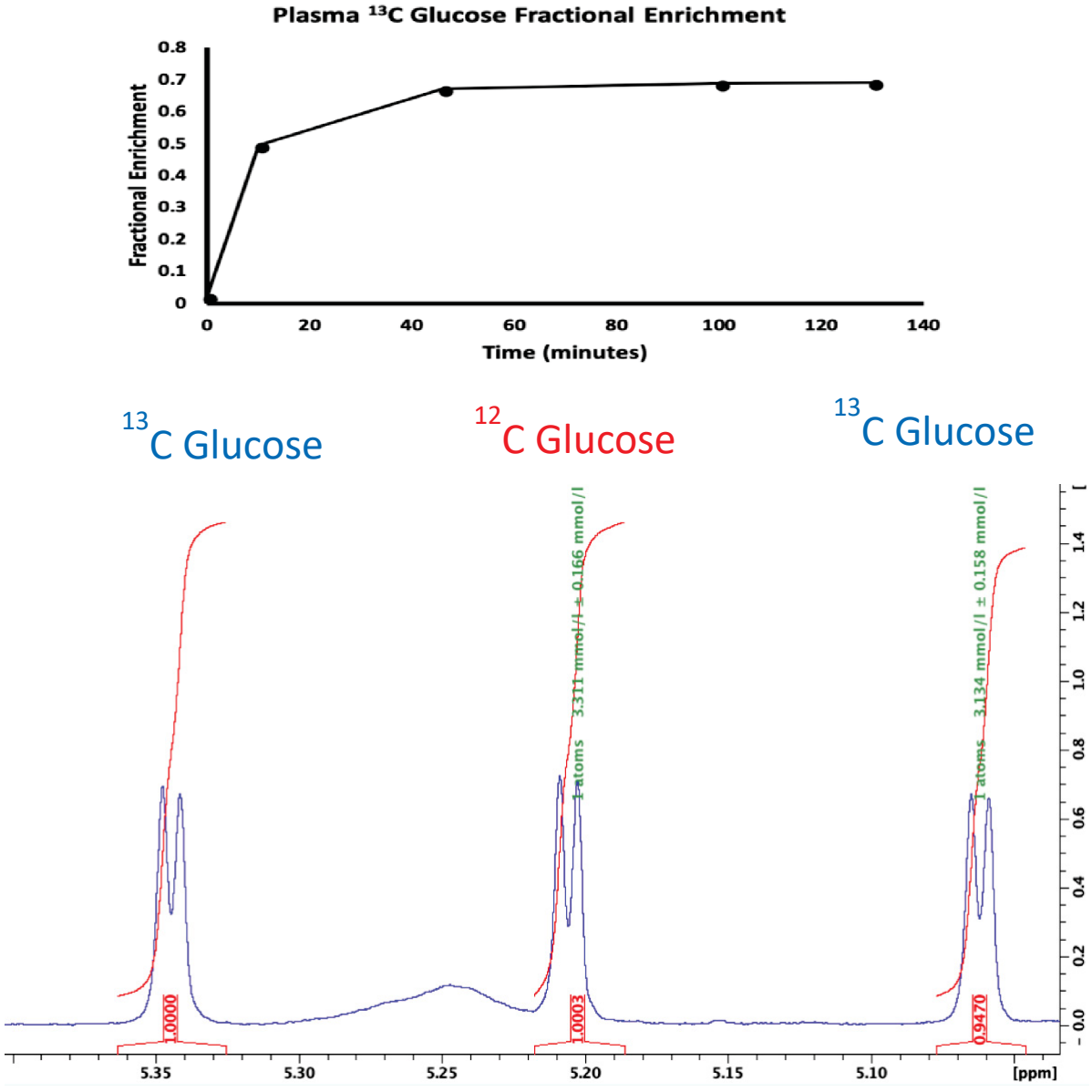

Figure 6: *Processing of plasma MRS spectra and $_{13}C$ fractional enrichment*
Plasma NMR data was analyzed using Bruker TopSpin program. Protons attached to $_{12}$Carbon-6 of alpha D-glucose resonates at 5.22 ppm, however if the sixth position carbon is $_{13}$C, satellite peaks will appear at 5.06 and 5.34 ppm. Glucose fractional enrichment was obtained by using the peak integration tool and dividing the signal of the $_{13}$C satellite peaks over the sum of both H-$_{13}$C and H-$_{12}$C signals. Molar concentrations of plasma glucose were calculated using a 5nM benzoic acid reference.

reference to calculate molar concentrations. A 1D-CPMG (Carr-Purcell-Meiboom-Gill) sequence was used to filter out the signal from macromolecules which normally create broad signals in the background with sequences (such as 1D-NOESY) which do not use T2 filters. Negligible broad lipoprotein contamination can be seen at 5.25 ppm.

3.5 Quantification and Modelling of in vivo spectra

Processing of the in-vivo MR spectra was performed in MATLAB using the FID-A toolkit and consisted of a retrospective phase and frequency drift correction and zero padding[98]. Edit-ON and edit-OFF scans were then separately averaged and aligned before subtraction. LCModel was used for analyzing the spectra using two in-house simulated basis sets: one for standard ^{1}H metabolites which was used to fit the edit OFF spectra, and one for selected ^{13}C enriched metabolites which was used to fit the POCE difference spectra.

Fractional enrichment (FE) was calculated using LCModel estimates of the concentration of label ^{13}C in the metabolite divided by the summed concentrations of ^{13}C and ^{12}C in the metabolite.

$$FE\ C_i = \frac{^{13}C\ concentration\ in\ C_i}{(^{13}C + 12C)\ concentration\ in\ C_i}$$

The time courses of [4-^{13}C]-glutamate and [4-^{13}C]-glutamine FE were then calculated by dividing the amount of labelled signal by the total concentration of glutamate and glutamine at each time point respectively. The fractional enrichment of these metabolites can then be used in metabolic modelling to calculate the rate of labeling as a measurement of metabolic flux.

Modelling of spectral timeseries data and flux calculations were also performed in MATLAB using a series of mass and ^{13}C isotope balance equations describing ^{13}C labeling in neurons from previous literature[99].

Glucose transport across the blood brain barrier:

$$\frac{d}{dt}[Glc(t)b] = Tmax\frac{\left([Glc(t)p] - \frac{[Glc(t)b]}{Vd}\right)}{Kt + \frac{[Glc(t)b]}{Vd} + [Glc(t)p]} - CMRGlc$$

Lactate

$$\frac{d}{dt}[Lac] = CMRGlc\left(\frac{Glcb1 + Glcb6}{[Glc]}\right) - (Vout + Vtca)\left(\frac{Lac3}{[Lac]}\right) + (Vin * FELac1)$$

Aspartate

$$\frac{d}{dt}[Asp] = Vx\left(\frac{OAA2}{[OAA]}\right) - Vx\left(\frac{Asp2}{[Asp]}\right)$$

Oxaloacetate

$$\frac{d}{dt}[OAA] = \frac{Vtca}{2}\left(\frac{OG3 + OG4}{[OG]}\right) + Vx\left(\frac{Asp2}{[Asp]}\right) - (Vx + Vtca)\left(\frac{OAA2}{[OAA]}\right)$$

Oxoglutarate

$$\frac{d}{dt}[OG] = Vtca\left(\frac{OAA2}{[OAA]}\right) + Vx\left(\frac{Glu3}{[Glu]}\right) - (Vx + Vtca)\left(\frac{OG4}{[OG]}\right)$$

Glutamate

$$\frac{d}{dt}[Glu] = Vx\left(\frac{OG3}{[OG]}\right) + Vnt\left(\frac{Gln3}{[Gln]}\right) - (Vx + Vtca)\left(\frac{Glu3}{[Glu]}\right)$$

Glutamine

$$\frac{d}{dt}[Gln] = Vnt\left(\frac{Glu3}{[Glu]}\right) - Vnt\left(\frac{Gln3}{[Gln]}\right)$$

A single-compartment neuronal metabolic model was fitted to the ^{13}C turnover curves from each of the three rat cohorts using a Levenberg-Marquardt algorithm. The decision to use a single-compartment model instead of a neuronal-glial model stemmed from several factors. Firstly, the two-compartment model requires the input of metabolic pools such as Glu and Gln C2, as well as aspartate and lactate to generate a complete model. These metabolites are non-resolvable using the indirect method at 7T, therefore more assumptions would have to be made to use the two-compartment model. Secondly, glucose metabolism is known to predominantly fuel the elevated neuronal energy demands, therefore a one-compartment neuronal model provides a thorough understanding into any alterations in glucose downstream metabolic pathways[100,101]. In fact, ^{1}H-[^{13}C] MRS has difficulty resolving Glu and Gln C3 at 7T, therefore by using a one compartment model we can sum their metabolic concentrations as Glx C3 in order to generate a more accurate model. The three fluxes that can be calculated using the three inputs (Glu C4, Gln C4, Glx C3) include the TCA cycle rate in the neuronal compartment (V_{TCA}), the flux through neuronal glutaminase from glutamate to glutamine (V_{NT}), and the rate of exchange from alpha-ketoglutarate to glutamate (V_X).

Several possible avenues were explored in how to best input the metabolite fractional enrichments into the model. First, we separately fitted each individual's FE curves to the metabolic model in order to obtain subject-specific estimates of V_{TCA}, V_{NT}, and V_X, which was used for statistical analysis. Total metabolic pool of glutamate, glutamine, aspartate, and lactate for each subject were obtained by averaging each subject's ^{1}H MRS concentrations over all time points and was used for references in metabolic modelling. A second avenue again fitted each individual's FE curves to the metabolic model, however the metabolic pool used in the model in this case were averaged across each cohort instead. Finally, both the FE curves and pool concentrations were

averaged for each cohort, and the average FE curve was fitted to the metabolic model to obtain a single estimate of V_{TCA}, V_{NT}, and V_X for each group (Figure 9). The three group FE curves were calculated by averaging the FE values at each time point across all animals within the same cohort. By averaging data within a cohort, the fluxes calculated will have a higher degree of confidence as noise or possible artifacts will be averaged out with the greater number of subjects. The robustness of the model was then verified using Monte Carlo simulations by adding random noise to the calculated flux values and seeing its effect on the standard deviation and degree of confidence for the estimated fluxes through five hundred iterations.

Finally, statistical testing was done using the SPSS statistics package. For comparison of ^1H metabolite concentrations in the brain between groups, a one-way multivariate analysis of variance (MANOVA) analysis was performed that included seven individual metabolites: total choline (GPC+PCh), N-acetyl aspartate (NAA), myo-inositol (Ins), Glutamate (Glu), Glutamine (Gln), and glutathione (GSH), and taurine (Tau). Post hoc Tukey test was performed to identify which cohorts differed. For comparison of metabolic fluxes, V_{TCA}, V_X, V_{NT}, between groups, a one-way ANOVA was performed on the individual flux rates, followed by post hoc Tukey test to identify the significant differences.

Chapter 4: Results

4.1 Time Series Spectra

Figure 7 shows an example of a typical ^{1}H-[^{13}C] MRS time series acquired throughout the two-hour scan duration. The S/N of ^{13}C edited NMR spectra is 16, and the glutamate/glutamine-C2 peak can be seen at 3.7 ppm in a similar enrichment to glutamate/glutamine-C3 peak. The carrier frequency of ^{13}C nucleus was centered at 35 ppm. At baseline pre-infusion, almost no ^{13}C labeling can be seen, and the signal is mostly due to noise. As the infusion begins, a gradual increase of ^{13}C

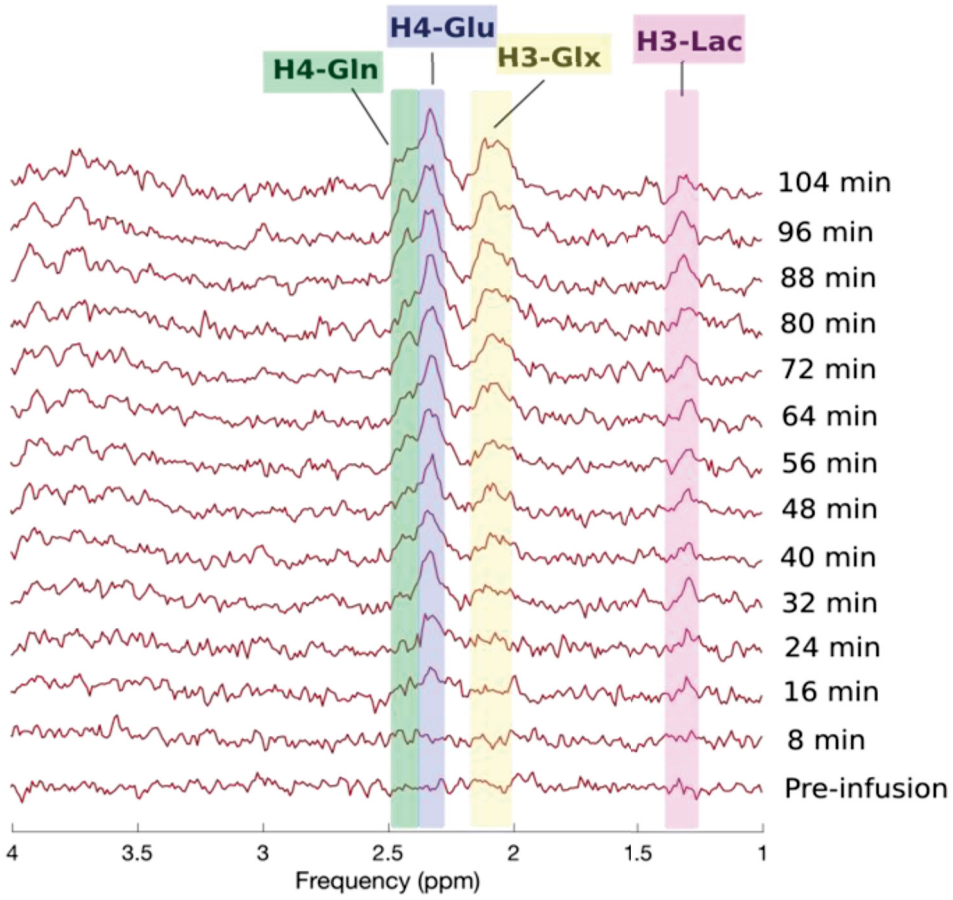

Figure 7*: Sample of 1H-[13C] MRS time series data over an experimental duration*

labelled proton signal for the 4th carbon of glutamate (2.35 ppm) and glutamine (2.45 ppm) as well as their 3rd carbon (2.1 ppm) can be seen over the course of the scan session. Since we are unable to separately resolve the 3rd carbon peaks of glutamate and glutamine, they were summed

and labelled as Glx. Similarly, the peak for lactate, further downstream in glucose metabolism, can be seen slightly increasing at 1.3ppm.

4.2 ^{1}H MRS

Seven neurometabolites commonly associated with dementia and neurodegenerative diseases were compared between the three cohorts using SPSS statistical analysis software (Fig 8).

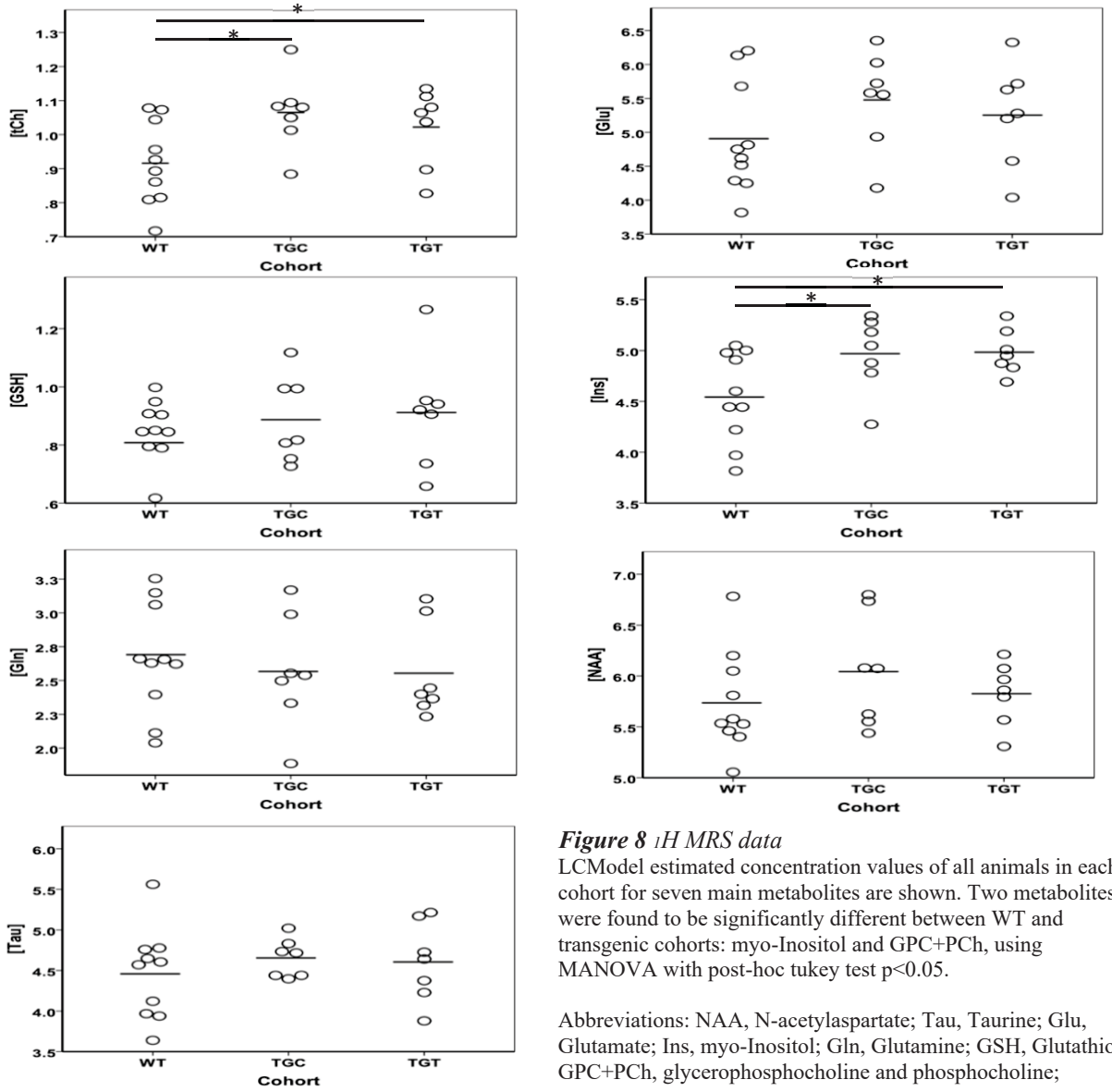

Figure 8 *^{1}H MRS data*
LCModel estimated concentration values of all animals in each cohort for seven main metabolites are shown. Two metabolites were found to be significantly different between WT and transgenic cohorts: myo-Inositol and GPC+PCh, using MANOVA with post-hoc tukey test $p<0.05$.

Abbreviations: NAA, N-acetylaspartate; Tau, Taurine; Glu, Glutamate; Ins, myo-Inositol; Gln, Glutamine; GSH, Glutathione; GPC+PCh, glycerophosphocholine and phosphocholine;

Estimated concentrations were taken from water referenced LCModel output and averaged across all subjects within each cohort. A multivariate analysis of variance with Tukey Post-hoc revealed a significant difference between myo-Inositol (Ins) levels between the wild type and transgenic control as well as between wild type and transgenic treated $p<0.01$. Specifically, Ins levels were found to be elevated in both untreated and treated transgenic animals relative to wild type animals. This finding is in line with previous MRS studies in both AD patients and rodent models of AD, in which elevated Ins is commonly observed and is believed to reflect neuroinflammation. Similarly, there was a significant increase in GPC+PCh concentrations in transgenic control animal relative to wild type animals ($p<0.05$), but no significant difference was seen between wild type and transgenic treated. This finding may suggest that elevated GPC+PCh levels is associated with AD pathology, and that early treatment with anti-inflammatory drugs can reverse this change. Increased GPC+PCh levels are hypothesized to represent a decrease in cellular membrane integrity and has been seen in previous AD literature[102].

4.3 ^{13}C MRS

Fractional enrichment plots revealed the dynamics of label uptake in both Glu-H4 and Gln-H4, as well as Glx-H3 for the three different cohorts (Fig 9). A comparison between the ^{13}C fractional enrichment of the three groups show that wild type rats achieve a 40% fractional enrichment in ^{13}C Glu-C4 labeling by 60 minutes whereas the transgenics only reach the same level of fractional enrichment by 80 minutes. Similarly, the labeling curve for Gln-C4 reaches 20% FE by 60 minutes but transgenics reach the same level at 80 minutes. Finally, for labelling of Glx-C3, wild types reach 20% FE by 40 minutes whereas transgenics took 60 minutes. Near the end of the time course, the fractional enrichment of Glx-C3 can be seen to exceed the fractional enrichment of Glu-C4, which is in agreement with a few previous studies from literature[103-105]. One compartment

metabolic modelling of the fractional enrichment data for all three cohorts was performed to fit the experimental values (Fig 9).

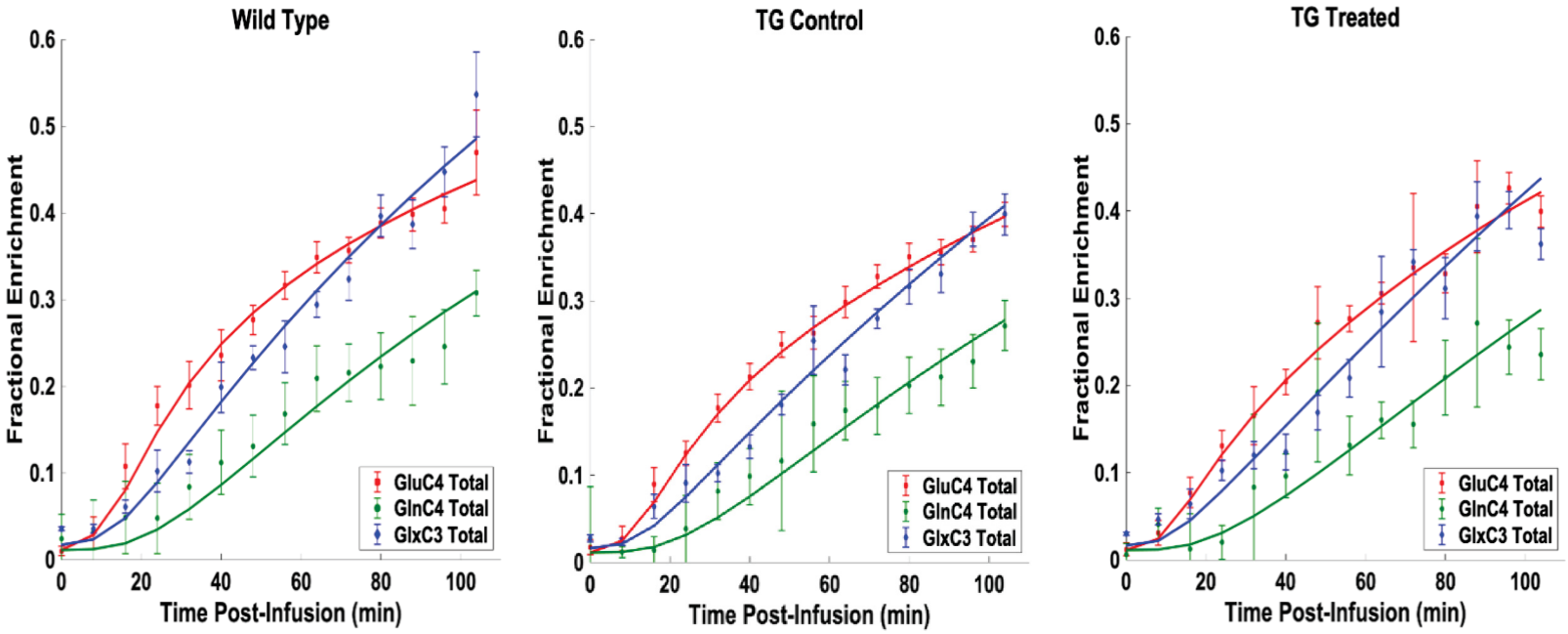

Figure 9 *Fractional Enrichment and Fluxes*
Fractional enrichment rates of the average data for the three cohorts are shown (Wild type n=11, TG control n=7, TG treated n=8. Fluxes calculated for each cohort is shown after fitting with a one compartment metabolic model.

Table 1

Modelled Fitted Flux Rates

Cohort	V_{TCA} (µmol/g/min)	V_{NT} (µmol/g/min)	V_X (µmol/g/min)
Wild Type (n=11)	0.58 ± 0.05	0.058 ± 0.005	0.25 ± 0.03
TG Control (n=7)	0.52 ± 0.04	0.060 ± 0.004	0.22 ± 0.02
TG Treated (n=8)	0.48 ± 0.07	0.052 ± 0.006	0.15 ± 0.02

The flux values for V_{TCA}, V_{NT}, and V_X were determined for wild type rats to be 0.58, 0.06, and 0.25μmol/g/min respectively, in good agreement results from previous literature[86,91] (Table 1). Transgenic control rats with AD pathology showed a significant decrease in V_{TCA} cycle as well as V_X compared to their wild type counterparts with 0.52 and 0.22 respectively, $p<0.05$. Furthermore, transgenic rats treated with Naproxen showed further deterioration with even lower V_{TCA} and V_X values of 0.48 and 0.15. No significant changes were seen between cohorts for rate of neurotransmission V_{NT}.

4.4 Monte Carlo Simulations

Monte Carlo simulations with 500 iterations were performed on each cohort to verify the validity of the model. The distribution of resulting fluxes after giving random noise to the fractional enrichments were graphed in a histogram (Fig 10). All three fluxes for each of the three cohorts display a normal distribution with small dispersion, centered around the estimated flux value. The resulting flux estimates were not significantly different when compared to the values after initial metabolic fitting to the model, demonstrating that the model is adequately robust (Table 2).

Table 2

Monte Carlo Simulated Fluxes

N=500	V_{TCA} (μmol/g/min)	V_{NT} (μmol/g/min)	V_X (μmol/g/min)
Wild Type	0.56 ± 0.02	0.060 ± 0.003	0.24 ± 0.01
TG Control	0.52 ± 0.03	0.061 ± 0.003	0.22 ± 0.02
TG Treated	0.46 ± 0.06	0.053 ± 0.006	0.14 ± 0.01

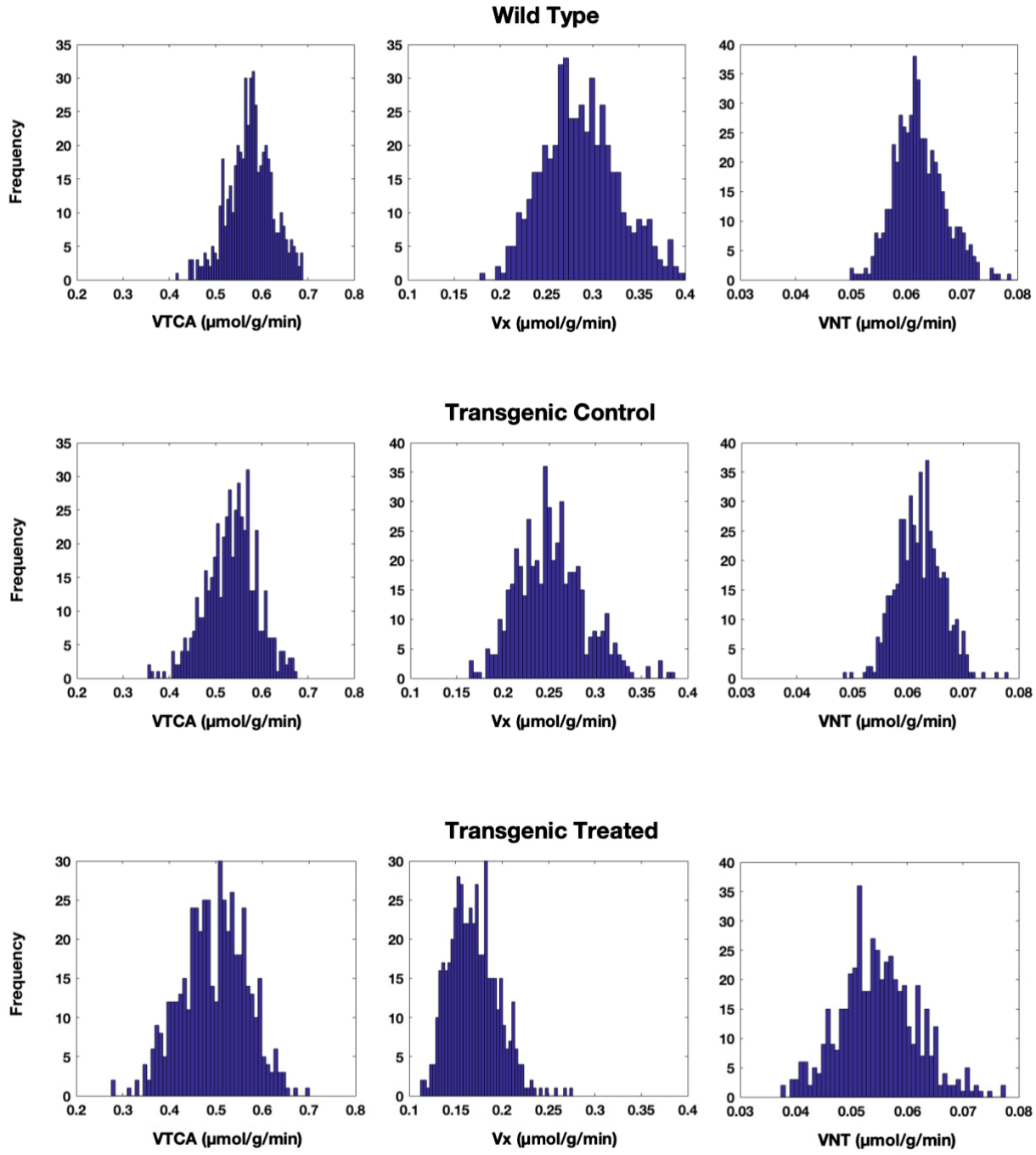

Figure 10 *Monte Carlo Simulation Histograms*
A 500 iteration Monte Carlo simulation was performed by adding random noise to the fractional enrichments of all three cohorts. The resulting histograms of the flux frequency distributions show a normal distribution with small dispersion, demonstrating strong reliability of the model.

Chapter 5: Discussion

To date, altered brain metabolism in Alzheimer's disease has not been examined extensively in vivo using ^{13}C MRS. The present study has shown for the first-time successful measurement of ^{13}C labeling in the TgF344-AD rat model of AD, as well as quantitative analysis of metabolic rates. Memory and Aβ plaque load was not measured directly in the current study, however according to initial descriptions of the animal model, TgF344-AD rats exhibit significant behavioral deficits in memory related tasks as well as significant amyloid plaque load by the 15 months time point[66].

5.1 ^{1}H MRS

Seven metabolites of interest from previous literature were chosen for analysis due to their roles in AD pathology as well as the sufficient quality of their spectral peaks using a quantitative cut off of 15% Cramér–Rao lower bounds error given by LCModel using water referenced concentrations. These include N-acetylaspartate (NAA), taurine (Tau), glutamate (Glu), myo-Inositol (Ins), glutamine (Gln), glutathione (GSH), and glycerophosphocholine with phosphocholine (GPc + PCh). ^{1}H MRS spectra showed that both control transgenics and Naproxen treated transgenics had elevated levels of Ins compared to wild type.

Ins

The finding of increased Ins levels in transgenic AD rats relative to wild type controls is consistent with previous literature and has repeatedly been replicated MRS studies of AD[106,107]. The neurobiological significance of this increase is still under debate. As myo-Inositol is associated with glial cells, the increase is hypothesized to be a response to increased astrogliosis in AD, which secretes neurotoxic pro-inflammatory cytokines[108]. Interestingly, the increase in Ins has also been shown to occur in asymptomatic at-risk individuals prior to dementia onset, making it a potentially early non-invasive biomarker[109]. There were no significant differences in Ins levels

between the Naproxen treated and the non-treated transgenic cohorts which challenges the role of neuroinflammation in AD pathology. It is possible that since Naproxen treatment is stopped at 10 months of age, there were no long-lasting carry over effects present by the 16-month time point.

GPC + PCh

A significant difference was also seen in total choline levels with untreated transgenics showing significantly increased levels compared to wild type cohorts, consistent with previous literature findings[102]. The choline peak represents glycerophosphocholine (GPC) and phosphocholine (PCh), breakdown products of phosphatidylcholine which is predominantly found in cellular membranes. The increase in choline peak could signify an increase in the breakdown of cellular membranes, contributing to cell loss in AD[110]. Interestingly, the naproxen treated group had significantly lower GPC+PCh levels compared with untreated transgenic rats, suggesting that early treatment with Naproxen may reduce pathological elevation of total choline levels and that this reduction may persist beyond the cessation of treatment.

NAA

Two important negative findings could also be seen from the ^{1}H MRS data. Firstly, there was no difference in concentration of NAA between all three cohorts. Previous ^{1}H MRS studies have repeatedly found a significant decrease in NAA levels, representing lowered neuronal density and integrity in AD pathology[36,111,112]. However, consistent with the current study, at least one recent study also failed to detect any differences in NAA levels in AD patients and animal models[113]. It is possible that since neuronal death is a late-stage symptom, it has not occurred by the 16-month time point in the TgF344-AD rat model, resulting in no NAA level differences. However, this seems highly unlikely as this rat model exhibits full blown AD pathology by this time point, with visible amyloid plaques, NFTs, and behavioral deficits. Additionally, this rat

model is reported to have 33% neuronal loss by the 16-month time point in its initial publication. While NAA is generally accepted to be a marker of neuronal viability, some evidence argues that NAA is not sensitive to neuronal density but rather to cellular dysfunction due to mitochondrial dysfunction, which has been shown to occur in AD, however this finding is controversial[114]. As the TgF344-AD model is the first rodent AD model to exhibit tau pathology naturally without human mutated tau genes, it is possible that NAA levels correspond differently to neuronal density and that mitochondrial dysfunction may be delayed due to endogenous compensatory or protective mechanisms.

Glu + Gln

Secondly, we detected no significant difference in glutamate and glutamine levels between the three experimental cohorts. However, glutamate levels exhibited a trend towards significance ($p<0.08$), showing increased glutamate levels in the transgenic cohorts compared to wild type. The literature findings on glutamate levels in AD have been varied, with findings that show reductions, increases, or no change. However, the majority of in vivo MRS studies have shown a reduction in glutamate and glutamine levels in AD[115,116]. Contrary to our findings, the leading hypothesis is that as a result of neuronal damage and loss in AD, the impacted brain regions will have lowered glutamatergic activity, causing a decrease in glucose metabolic rates and the synthesis of downstream metabolites glutamate and glutamine. As these metabolites are closely related to the bioenergetics and metabolism of glucose in the brain, their ^{1}H MRS concentration findings will be looked at in tandem with the ^{13}C MRS results.

5.2 ^{13}C MRS

Referring back to Figure 1, three fluxes of interest were analyzed in the glucose metabolism pathway. Specifically, we found that the transgenic cohorts had significantly reduced TCA cycle flux, V_{TCA}, and reduced rate of exchange between alpha ketoglutarate and glutamate, Vx, when compared to wild types. While previous studies have examined TCA cycle flux, neurotransmitter cycle and Vx in ex-vivo tissue, the present study is the first in vivo study to quantitatively identify specific downstream mechanisms that explain the decrease in glucose metabolism in the TgF344-

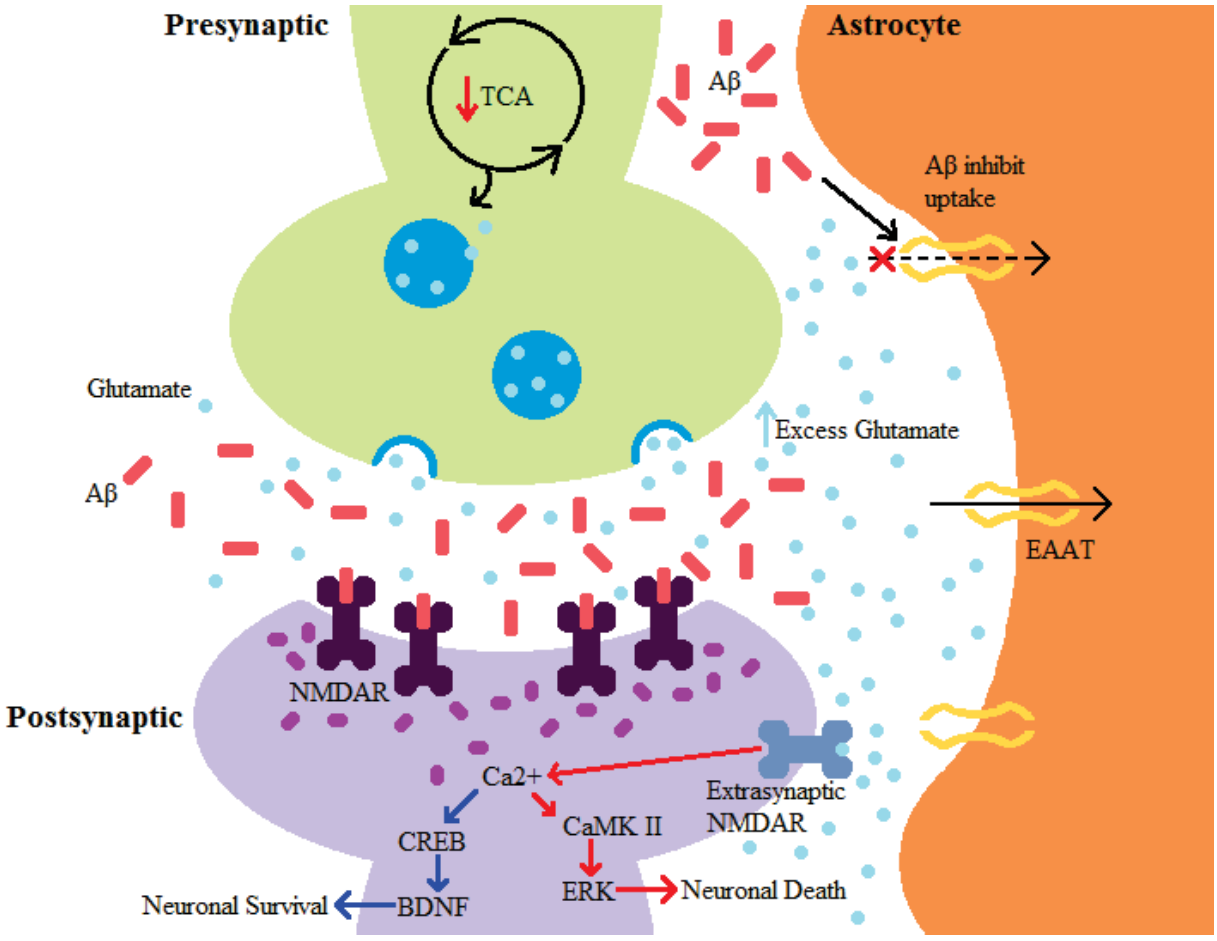

Figure 11: *Proposed model of glutamate mediated excitotoxicity*
Aβ blocks post-synaptic NMDA receptors and astroglial EAAT activity resulting in an increase of glutamate at the synapse. Excess glutamate activates extrasynaptic NMDA receptors causing calcium-mediated excitotoxicity and activation of CaMK II mediated neuronal cell death pathways.

Abbreviations: TCA, tricarboxylic acid cycle; NMDAR, N-methyl-D-aspartate receptor; EAAT, excitatory amino acid transporter; CREB, cAMP response element-binding protein; BDNF, brain-derived neurotrophic factor; CaMK II, Ca^{2+}/calmodulin-dependent protein kinase II; ERK, extracellular signal-regulated kinases.

AD model. Our findings of changes in glucose metabolism in AD provide a more comprehensive look on current glutamate-mediated toxicity theories of AD as shown in Figure 11.

Glutamatergic neurons have been shown to be sensitive to Aβ toxicity[117]. Specifically, elevated levels of Aβ blocks typical neuronal glutamate uptake at the synaptic cleft and disrupts calcium homeostasis in postsynaptic neurons resulting in the inactivation of cellular survival pathways and promoting pathways involved in hyperphosphorylation of tau[118].

Our ^{1}H MRS and ^{13}C MRS findings show that despite impaired labelling of glutamate via the TCA cycle representing decreased de-novo glutamate synthesis, the total cerebral glutamate pool concentration remains unchanged. In fact, our ^{1}H MRS show that glutamate levels trend towards a significant increase in the transgenic cohorts instead, hinting at a reduction in glutamate reuptake and glutamate metabolism, resulting in an excess of glutamate trapped in the synaptic cleft. However, this speculation requires further testing as the extracellular pool of glutamate contributes poorly to the overall pool size when compared to the intracellular pool, therefore it is hard to comment on its contribution to glutamate uptake based on measurements of the total glutamate pool. Other studies have indeed shown reduced expression of glutamate reuptake transporters such as the excitatory amino acid transporter (EAAT) have been seen in AD brains, indicative of lowered glutamate metabolism[119,120]. In vitro studies using species of Aβ peptides in cell culture also support the idea that toxic Aβ may allow for more glutamate availability by impairing astroglial glutamate uptake/recycling mechanisms[121].

This enhanced glutamate supply is likely to contribute to AD-associated excitotoxicity and neurodegeneration[33]. Normally, post-synaptic calcium signaling activates cellular transcription factors such as cAMP response element-binding protein (CREB) which regulates transcription of brain-derived neurotrophic factor (BDNF), a neuronal growth factor that helps support survival of

neurons[122]. However, the synaptic increase of Aβ in AD disrupts glutamate-mediated neurotransmission by blocking post-synaptic NMDA receptors and causes an excess of glutamate at the synapse. Excess glutamate spills over and activate nearby extrasynaptic NMDA receptors that trigger a sequence of intracellular events resulting in excessive calcium influx and activating calcium/calmodulin-dependent protein kinase II (CaMKII) neuronal cell death pathways[123]. This process is well documented and is the rationale behind Memantine, an NMDA receptor antagonist, as a potential treatment in AD[124,125]. It is possible that previous ^{1}H MRS findings of decreased glutamate levels in animal models and humans captured the final pathological events of neuronal loss, while our findings more closely replicate the mechanisms of neuronal excitotoxicity caused by glutamate resulting in neurodegeneration in the earlier stages of AD.

Finally, we found no significant difference in the apparent neurotransmission rate (V_{NT}) between transgenic and wild type cohorts, which contradicts the hypothesis of reduced astroglial reuptake of glutamate from the synapse. However, the reliability of this finding is questionable, as the flux rate is on a factor of 10 times smaller than V_{TCA}, increasing its sensitivity to error especially with a limited sample size. Furthermore, as mentioned previously, flux rates were modelled using a one compartment model that focused on the neuronal TCA cycle and glutamine is considered as one total pool. As such, V_{NT} modelling considered both glial and neuronal components of glutamine, rather than the glial component alone from glutamine synthetase activity after glutamate reuptake.

Treatment with Naproxen showed no effect in rescuing any of the three flux rates identified in the transgenic cohort. These findings are in agreement with our ^{1}H MRS data, where myo-Inositol levels did not differ between treated transgenics and transgenic control. Although the lack of effect may stem from issues with dosage or postponed scanning 6 months after treatment was

stopped, human clinical trial data also show no benefit of Naproxen treatment when compared to placebo, therefore lacks promise as a potential therapeutic option[126,127]. That being said, epidemiological data on the neuroprotective effects of NSAIDs is too strong to simply ignore[128], and the effects of neuroinflammation in AD cannot be ruled out with the failure of Naproxen treatment alone; different types of NSAIDs with diverging targets should be investigated in order to identify the specific cytokines and inflammatory pathway involved in AD.

5.3 Limitations and future directions

One of the major limitations in ^{13}C MRS experiments, or studies of cerebral energetics in general is that the effect of anesthesia must be considered. Most commonly used anesthesia including sevoflurane and isoflurane, used in the current study, are known to cause reductions in cerebral metabolic rates which would directly impact studies looking to investigate changes in metabolism in diseased populations. In the present study, this limitation is partially controlled for as all three cohorts experienced the same level of anesthesia, and their metabolic flux values were compared to each other rather than stated as an absolute truth. However, future directions must establish well-developed protocols for the MRS measurements performed in awake animals, in order for any metabolite concentration and metabolic flux values to be reliable as biomarkers for AD. Development of these procedures would also facilitate how translatable these methods are in human research. A second limitation of our experimental protocol was that although the animals were heated using warm air throughout the scan duration, their body temperatures were not measured, and therefore could be a factor in the resulting measurements. Future studies should involve precise monitoring and control of the animal's body temperature. A third limitation was touched on briefly, in that this experimental set up was not designed to capture the glial component of cerebral glucose metabolism and particularly the levels of glutamine in the brain. Future

direction would be to perform ^{13}C labeled acetate infusion which will predominantly undergo uptake by glial cells and paint a more complete picture of the full metabolism in the TgF344-AD rat model.

Future studies should aim to repeat the present study at multiple time points, in order to better understand the development of metabolism changes through disease progression. Furthermore, this will allow us to look at how metabolic changes correlate with other markers of AD such as amyloid beta deposition and NFT development. Similarly, as anatomical MRI scans are performed for MRS voxel placement, longitudinal structural data can be analyzed to identify cerebral atrophy correlated with AD progression. Finally, future studies should aim to increase the sample size per cohort to increase statistical power to verify the validity of trends towards significance such as in the case of glutamate levels.

Chapter 6: Conclusion

Here, we demonstrated that ^{13}C MRS can reveal, *in vivo*, alterations in specific glucose metabolism pathways in AD. ^{1}H MRS data showed a significant difference between AD transgenics and wild type in levels of myo-Inositol and phosphocholines, with Naproxen treatment having no lasting effect on Ins levels, but some lasting effect on GPC+PCh levels. NAA and glutamate levels have been shown to not exhibit change in the TgF344-AD model. Furthermore, cerebral metabolic flux is shown to be directly detectable in vivo in this rat model. Specifically, we found that transgenic AD rats exhibited slower V_{TCA} and V_X fluxes when compared to wildtype. This is in accordant with our first hypothesis. The decreased V_{TCA} measured is consistent with previous PET-based literature of hypometabolism in these regions. The confirmation of altered TCA cycle flux could serve as a biomarker for AD and allow for developments of treatment approaches to target this metabolic pathway. The flux rates also showed that transgenic rats with early Naproxen treatment did not demonstrate any carry over therapeutic benefit over non-treated transgenics contrary to our hypothesis, suggesting that either prolonged Naproxen treatment is necessary or that the metabolic impairments observed in AD are not linked to neuroinflammation. These findings indicate further research should be done on Naproxen's mechanism of action and its role in neuroinflammation in the AD context. We expect both our experimental methods and findings to be translatable to humans and that translational ^{1}H and ^{13}C MRS methods will allow for early detection of decreased glucose metabolism in pre-symptomatic stages of AD.

References

1 Nichols, E. *et al.* Global, regional, and national burden of Alzheimer's disease and other dementias, 1990–2016: a systematic analysis for the Global Burden of Disease Study 2016. *The Lancet Neurology* **18**, 88-106, doi:10.1016/S1474-4422(18)30403-4 (2019).

2 Qiu, C., Kivipelto, M. & von Strauss, E. Epidemiology of Alzheimer's disease: occurrence, determinants, and strategies toward intervention. *Dialogues in clinical neuroscience* **11**, 111-128 (2009).

3 Kirson, N. Y. *et al.* Assessing the economic burden of Alzheimer's disease patients first diagnosed by specialists. *BMC geriatrics* **16**, 138-138, doi:10.1186/s12877-016-0303-5 (2016).

4 Fernández, M., Gobartt, A. L., Balañá, M. & the, C. S. G. Behavioural symptoms in patients with Alzheimer's disease and their association with cognitive impairment. *BMC Neurology* **10**, 87, doi:10.1186/1471-2377-10-87 (2010).

5 Helzner, E. P. *et al.* Survival in Alzheimer disease: a multiethnic, population-based study of incident cases. *Neurology* **71**, 1489-1495, doi:10.1212/01.wnl.0000334278.11022.42 (2008).

6 Guerreiro, R. & Bras, J. The age factor in Alzheimer's disease. *Genome medicine* **7**, 106-106, doi:10.1186/s13073-015-0232-5 (2015).

7 Mohandas, E., Rajmohan, V. & Raghunath, B. Neurobiology of Alzheimer's disease. *Indian journal of psychiatry* **51**, 55-61, doi:10.4103/0019-5545.44908 (2009).

8 Näslund, J. *et al.* Correlation Between Elevated Levels of Amyloid β-Peptide in the Brain and Cognitive Decline. *JAMA* **283**, 1571-1577, doi:10.1001/jama.283.12.1571 (2000).

9 Pauwels, K. *et al.* Structural basis for increased toxicity of pathological abeta42:abeta40 ratios in Alzheimer disease. *J Biol Chem* **287**, 5650-5660, doi:10.1074/jbc.M111.264473 (2012).

10 Dekker, A. D., Fortea, J., Blesa, R. & De Deyn, P. P. Cerebrospinal fluid biomarkers for Alzheimer's disease in Down syndrome. *Alzheimer's & Dementia: Diagnosis, Assessment & Disease Monitoring* **8**, 1-10, doi:https://doi.org/10.1016/j.dadm.2017.02.006 (2017).

11 Reiss Allison, B., Arain Hirra, A., Stecker Mark, M., Siegart Nicolle, M. & Kasselman Lora, J. in *Reviews in the Neurosciences* Vol. 29 613 (2018).

12 Kuperstein, I. *et al.* Neurotoxicity of Alzheimer's disease Aβ peptides is induced by small changes in the Aβ42 to Aβ40 ratio. *The EMBO journal* **29**, 3408-3420, doi:10.1038/emboj.2010.211 (2010).

13 Demuro, A., Parker, I. & Stutzmann, G. E. Calcium signaling and amyloid toxicity in Alzheimer disease. *J Biol Chem* **285**, 12463-12468, doi:10.1074/jbc.R109.080895 (2010).

14 Morgan, D. *et al.* Aβ peptide vaccination prevents memory loss in an animal model of Alzheimer's disease. *Nature* **408**, 982-985, doi:10.1038/35050116 (2000).

15 Panza, F. *et al.* Are antibodies directed against amyloid-β (Aβ) oligomers the last call for the Aβ hypothesis of Alzheimer's disease? *Immunotherapy* **11**, 3-6, doi:10.2217/imt-2018-0119 (2018).

16 Selkoe, D. J. Alzheimer disease and aducanumab: adjusting our approach. *Nature Reviews Neurology* **15**, 365-366, doi:10.1038/s41582-019-0205-1 (2019).
17 Rodrigue, K. M., Kennedy, K. M. & Park, D. C. Beta-amyloid deposition and the aging brain. *Neuropsychology review* **19**, 436-450, doi:10.1007/s11065-009-9118-x (2009).
18 Bennett, D. A. *et al.* Neuropathology of older persons without cognitive impairment from two community-based studies. *Neurology* **66**, 1837-1844, doi:10.1212/01.wnl.0000219668.47116.e6 (2006).
19 Aizenstein, H. J. *et al.* Frequent amyloid deposition without significant cognitive impairment among the elderly. *Archives of neurology* **65**, 1509-1517, doi:10.1001/archneur.65.11.1509 (2008).
20 Ittner, L. M. & Götz, J. Amyloid-β and tau — a toxic pas de deux in Alzheimer's disease. *Nature Reviews Neuroscience* **12**, 67, doi:10.1038/nrn2967 (2010).
21 Oddo, S., Caccamo, A., Kitazawa, M., Tseng, B. P. & LaFerla, F. M. Amyloid deposition precedes tangle formation in a triple transgenic model of Alzheimer's disease. *Neurobiology of Aging* **24**, 1063-1070, doi:https://doi.org/10.1016/j.neurobiolaging.2003.08.012 (2003).
22 Oddo, S., Billings, L., Kesslak, J. P., Cribbs, D. H. & LaFerla, F. M. Aβ Immunotherapy Leads to Clearance of Early, but Not Late, Hyperphosphorylated Tau Aggregates via the Proteasome. *Neuron* **43**, 321-332, doi:https://doi.org/10.1016/j.neuron.2004.07.003 (2004).
23 Tseng, B. P., Green, K. N., Chan, J. L., Blurton-Jones, M. & LaFerla, F. M. Abeta inhibits the proteasome and enhances amyloid and tau accumulation. *Neurobiology of aging* **29**, 1607-1618, doi:10.1016/j.neurobiolaging.2007.04.014 (2008).
24 Rodríguez-Martín, T. *et al.* Tau phosphorylation affects its axonal transport and degradation. *Neurobiology of aging* **34**, 2146-2157, doi:10.1016/j.neurobiolaging.2013.03.015 (2013).
25 Jankowsky, J. L. & Zheng, H. Practical considerations for choosing a mouse model of Alzheimer's disease. *Molecular neurodegeneration* **12**, 89-89, doi:10.1186/s13024-017-0231-7 (2017).
26 Braak, H., Zetterberg, H., Del Tredici, K. & Blennow, K. Intraneuronal tau aggregation precedes diffuse plaque deposition, but amyloid-beta changes occur before increases of tau in cerebrospinal fluid. *Acta Neuropathol* **126**, 631-641, doi:10.1007/s00401-013-1139-0 (2013).
27 Bejanin, A. *et al.* Tau pathology and neurodegeneration contribute to cognitive impairment in Alzheimer's disease. *Brain* **140**, 3286-3300, doi:10.1093/brain/awx243 (2017).
28 Iaccarino, L. *et al.* Local and distant relationships between amyloid, tau and neurodegeneration in Alzheimer's Disease. *NeuroImage. Clinical* **17**, 452-464, doi:10.1016/j.nicl.2017.09.016 (2017).
29 Mergenthaler, P., Lindauer, U., Dienel, G. A. & Meisel, A. Sugar for the brain: the role of glucose in physiological and pathological brain function. *Trends in neurosciences* **36**, 587-597, doi:10.1016/j.tins.2013.07.001 (2013).
30 Cunnane, S. *et al.* Brain fuel metabolism, aging, and Alzheimer's disease. *Nutrition (Burbank, Los Angeles County, Calif.)* **27**, 3-20, doi:10.1016/j.nut.2010.07.021 (2011).

31 Coyle, J. T. & Puttfarcken, P. Oxidative stress, glutamate, and neurodegenerative disorders. *Science* **262**, 689, doi:10.1126/science.7901908 (1993).
32 Sheldon, A. L. & Robinson, M. B. The role of glutamate transporters in neurodegenerative diseases and potential opportunities for intervention. *Neurochemistry international* **51**, 333-355, doi:10.1016/j.neuint.2007.03.012 (2007).
33 Lewerenz, J. & Maher, P. Chronic Glutamate Toxicity in Neurodegenerative Diseases-What is the Evidence? *Frontiers in neuroscience* **9**, 469-469, doi:10.3389/fnins.2015.00469 (2015).
34 Grothe, M. J. *et al.* In vivo staging of regional amyloid deposition. *Neurology* **89**, 2031-2038, doi:10.1212/WNL.0000000000004643 (2017).
35 Mullins, R., Reiter, D. & Kapogiannis, D. Magnetic resonance spectroscopy reveals abnormalities of glucose metabolism in the Alzheimer's brain. *Annals of clinical and translational neurology* **5**, 262-272, doi:10.1002/acn3.530 (2018).
36 Graff-Radford, J. & Kantarci, K. Magnetic resonance spectroscopy in Alzheimer's disease. *Neuropsychiatric disease and treatment* **9**, 687-696, doi:10.2147/NDT.S35440 (2013).
37 Xu, J. *et al.* Graded perturbations of metabolism in multiple regions of human brain in Alzheimer's disease: Snapshot of a pervasive metabolic disorder. *Biochimica et biophysica acta* **1862**, 1084-1092, doi:10.1016/j.bbadis.2016.03.001 (2016).
38 Silverman, D. H. S. *et al.* Positron Emission Tomography in Evaluation of DementiaRegional Brain Metabolism and Long-term Outcome. *JAMA* **286**, 2120-2127, doi:10.1001/jama.286.17.2120 (2001).
39 Herholz, K. Cerebral glucose metabolism in preclinical and prodromal Alzheimer's disease. *Expert Rev Neurother* **10**, 1667-1673, doi:10.1586/ern.10.136 (2010).
40 Mosconi, L. *et al.* Multicenter standardized 18F-FDG PET diagnosis of mild cognitive impairment, Alzheimer's disease, and other dementias. *J Nucl Med* **49**, 390-398, doi:10.2967/jnumed.107.045385 (2008).
41 Anchisi, D. *et al.* Heterogeneity of brain glucose metabolism in mild cognitive impairment and clinical progression to Alzheimer disease. *Arch Neurol* **62**, 1728-1733, doi:10.1001/archneur.62.11.1728 (2005).
42 Caselli, R. J., Chen, K., Lee, W., Alexander, G. E. & Reiman, E. M. Correlating cerebral hypometabolism with future memory decline in subsequent converters to amnestic pre-mild cognitive impairment. *Arch Neurol* **65**, 1231-1236, doi:10.1001/archneurol.2008.1 (2008).
43 Brooks, L. G. & Loewenstein, D. A. Assessing the progression of mild cognitive impairment to Alzheimer's disease: current trends and future directions. *Alzheimer's research & therapy* **2**, 28-28, doi:10.1186/alzrt52 (2010).
44 Mosconi, L. Glucose metabolism in normal aging and Alzheimer's disease: Methodological and physiological considerations for PET studies. *Clinical and translational imaging* **1**, 10.1007/s40336-40013-40026-y, doi:10.1007/s40336-013-0026-y (2013).
45 Newcombe, E. A. *et al.* Inflammation: the link between comorbidities, genetics, and Alzheimer's disease. *Journal of Neuroinflammation* **15**, 276, doi:10.1186/s12974-018-1313-3 (2018).
46 Akiyama, H. *et al.* Inflammation and Alzheimer's disease. *Neurobiol Aging* **21**, 383-421 (2000).

47 Kitazawa, M., Oddo, S., Yamasaki, T. R., Green, K. N. & LaFerla, F. M. Lipopolysaccharide-induced inflammation exacerbates tau pathology by a cyclin-dependent kinase 5-mediated pathway in a transgenic model of Alzheimer's disease. *J Neurosci* **25**, 8843-8853, doi:10.1523/jneurosci.2868-05.2005 (2005).

48 Kaur, U. *et al.* Reactive oxygen species, redox signaling and neuroinflammation in Alzheimer's disease: the NF-kappaB connection. *Curr Top Med Chem* **15**, 446-457 (2015).

49 Solleiro-Villavicencio, H. & Rivas-Arancibia, S. Effect of Chronic Oxidative Stress on Neuroinflammatory Response Mediated by CD4(+)T Cells in Neurodegenerative Diseases. *Frontiers in cellular neuroscience* **12**, 114-114, doi:10.3389/fncel.2018.00114 (2018).

50 Navarro, V. *et al.* Microglia in Alzheimer's Disease: Activated, Dysfunctional or Degenerative. *Frontiers in aging neuroscience* **10**, 140-140, doi:10.3389/fnagi.2018.00140 (2018).

51 Heneka, M. T. *et al.* Neuroinflammation in Alzheimer's disease. *The Lancet Neurology* **14**, 388-405, doi:https://doi.org/10.1016/S1474-4422(15)70016-5 (2015).

52 Rapic, S. *et al.* Imaging microglial activation and glucose consumption in a mouse model of Alzheimer's disease. *Neurobiology of Aging* **34**, 351-354, doi:https://doi.org/10.1016/j.neurobiolaging.2012.04.016 (2013).

53 Moore, A. H. *et al.* Non-Steroidal Anti-Inflammatory Drugs in Alzheimer's Disease and Parkinson's Disease: Reconsidering the Role of Neuroinflammation. *Pharmaceuticals (Basel, Switzerland)* **3**, 1812-1841, doi:10.3390/ph3061812 (2010).

54 Choi, S. H. *et al.* Cyclooxygenase-1 inhibition reduces amyloid pathology and improves memory deficits in a mouse model of Alzheimer's disease. *J Neurochem* **124**, 59-68, doi:10.1111/jnc.12059 (2013).

55 Cryer, B. & Feldman, M. Cyclooxygenase-1 and Cyclooxygenase-2 Selectivity of Widely Used Nonsteroidal Anti-Inflammatory Drugs. *The American Journal of Medicine* **104**, 413-421, doi:10.1016/S0002-9343(98)00091-6 (1998).

56 Leoutsakos, J.-M. S., Muthen, B. O., Breitner, J. C. S., Lyketsos, C. G. & Team, A. R. Effects of non-steroidal anti-inflammatory drug treatments on cognitive decline vary by phase of pre-clinical Alzheimer disease: findings from the randomized controlled Alzheimer's Disease Anti-inflammatory Prevention Trial. *International journal of geriatric psychiatry* **27**, 364-374, doi:10.1002/gps.2723 (2012).

57 Benedikz, E., Kloskowska, E. & Winblad, B. The rat as an animal model of Alzheimer's disease. *Journal of cellular and molecular medicine* **13**, 1034-1042, doi:10.1111/j.1582-4934.2009.00781.x (2009).

58 Sasaguri, H. *et al.* APP mouse models for Alzheimer's disease preclinical studies. *The EMBO journal* **36**, 2473-2487, doi:10.15252/embj.201797397 (2017).

59 Yang, F., Uéda, K., Chen, P.-P., Ashe, K. H. & Cole, G. M. Plaque-associated α-synuclein (NACP) pathology in aged transgenic mice expressing amyloid precursor protein. *Brain Research* **853**, 381-383, doi:https://doi.org/10.1016/S0006-8993(99)02207-6 (2000).

60 Billings, L. M., Oddo, S., Green, K. N., McGaugh, J. L. & LaFerla, F. M. Intraneuronal Abeta causes the onset of early Alzheimer's disease-related cognitive deficits in transgenic mice. *Neuron* **45**, 675-688, doi:10.1016/j.neuron.2005.01.040 (2005).

61 Puzzo, D., Lee, L., Palmeri, A., Calabrese, G. & Arancio, O. Behavioral assays with mouse models of Alzheimer's disease: practical considerations and guidelines. *Biochemical pharmacology* **88**, 450-467, doi:10.1016/j.bcp.2014.01.011 (2014).

62 Drummond, E. & Wisniewski, T. Alzheimer's disease: experimental models and reality. *Acta neuropathologica* **133**, 155-175, doi:10.1007/s00401-016-1662-x (2017).

63 Hurtado, D. E. *et al.* A{beta} accelerates the spatiotemporal progression of tau pathology and augments tau amyloidosis in an Alzheimer mouse model. *The American journal of pathology* **177**, 1977-1988, doi:10.2353/ajpath.2010.100346 (2010).

64 Joshi, A., Ringman, J. M., Lee, A. S., Juarez, K. O. & Mendez, M. F. Comparison of clinical characteristics between familial and non-familial early onset Alzheimer's disease. *Journal of neurology* **259**, 2182-2188, doi:10.1007/s00415-012-6481-y (2012).

65 Oh, K.-J. *et al.* Staging of Alzheimer's Pathology in Triple Transgenic Mice: A Light and Electron Microscopic Analysis. *International Journal of Alzheimer’s Disease* **2010**, 24, doi:10.4061/2010/780102 (2010).

66 Cohen, R. M. *et al.* A transgenic Alzheimer rat with plaques, tau pathology, behavioral impairment, oligomeric aβ, and frank neuronal loss. *The Journal of neuroscience : the official journal of the Society for Neuroscience* **33**, 6245-6256, doi:10.1523/JNEUROSCI.3672-12.2013 (2013).

67 Kelleher, R. J., 3rd & Shen, J. Presenilin-1 mutations and Alzheimer's disease. *Proceedings of the National Academy of Sciences of the United States of America* **114**, 629-631, doi:10.1073/pnas.1619574114 (2017).

68 Rorabaugh, J. M. *et al.* Chemogenetic locus coeruleus activation restores reversal learning in a rat model of Alzheimer’s disease. *Brain* **140**, 3023-3038, doi:10.1093/brain/awx232 (2017).

69 Ross, B. D. *et al.* In vivo MR spectroscopy of human dementia. *Neuroimaging Clin N Am* **8**, 809-822 (1998).

70 Zhu, X. *et al.* Effects of Alzheimer disease on fronto-parietal brain N-acetyl aspartate and myo-inositol using magnetic resonance spectroscopic imaging. *Alzheimer disease and associated disorders* **20**, 77-85, doi:10.1097/01.wad.0000213809.12553.fc (2006).

71 Patel, A. B., Tiwari, V., Veeraiah, P. & Saba, K. Increased astroglial activity and reduced neuronal function across brain in AβPP-PS1 mouse model of Alzheimer’s disease. *Journal of Cerebral Blood Flow & Metabolism* **38**, 1213-1226, doi:10.1177/0271678X17709463 (2017).

72 Rodrigues, T., Valette, J. & Bouzier-Sore, A.-K. 13C NMR spectroscopy applications to brain energy metabolism. **5**, doi:10.3389/fnene.2013.00009 (2013).

73 Gruetter, R., Seaquist, E. R. & Ugurbil, K. A mathematical model of compartmentalized neurotransmitter metabolism in the human brain. *American Journal of Physiology-Endocrinology and Metabolism* **281**, E100-E112, doi:10.1152/ajpendo.2001.281.1.E100 (2001).

74 Henry, P.-G., Tkáč, I. & Gruetter, R. 1H-localized broadband 13C NMR spectroscopy of the rat brain in vivo at 9.4 T. *Magnetic Resonance in Medicine* **50**, 684-692, doi:10.1002/mrm.10601 (2003).

75 Lai, M. *et al.* In vivo 13C MRS in the mouse brain at 14.1 Tesla and metabolic flux quantification under infusion of [1,6-13C2]glucose. *Journal of Cerebral Blood Flow & Metabolism* **38**, 1701-1714, doi:10.1177/0271678X17734101 (2017).
76 Kumaragamage, C. *et al.* Minimum echo time PRESS-based proton observed carbon edited (POCE) MRS in rat brain using simultaneous editing and localization pulses. *Magnetic Resonance in Medicine* **80**, 1279-1288, doi:10.1002/mrm.27119 (2018).
77 Lanz, B., Gruetter, R. & Duarte, J. *Metabolic Flux and Compartmentation Analysis in the Brain In vivo*. Vol. 4 (2013).
78 Uffmann, K. & Gruetter, R. Mathematical modeling of 13C label incorporation of the TCA cycle: The concept of composite precursor function. *Journal of Neuroscience Research* **85**, 3304-3317, doi:10.1002/jnr.21392 (2007).
79 Henry, P.-G., Öz, G., Provencher, S. & Gruetter, R. Toward dynamic isotopomer analysis in the rat brain in vivo: automatic quantitation of 13C NMR spectra using LCModel. *NMR in Biomedicine* **16**, 400-412, doi:10.1002/nbm.840 (2003).
80 Shestov, A., Valette, J., Uğurbil, K. & Henry, P.-G. *On the reliability of 13C metabolic modeling with two-compartment neuronal-glial models*. Vol. 85 (2007).
81 Henry, P.-G. *et al.* In vivo 13C NMR spectroscopy and metabolic modeling in the brain: a practical perspective. *Magnetic Resonance Imaging* **24**, 527-539, doi:https://doi.org/10.1016/j.mri.2006.01.003 (2006).
82 Wyss, M. T., Magistretti, P. J., Buck, A. & Weber, B. Labeled acetate as a marker of astrocytic metabolism. *Journal of cerebral blood flow and metabolism : official journal of the International Society of Cerebral Blood Flow and Metabolism* **31**, 1668-1674, doi:10.1038/jcbfm.2011.84 (2011).
83 Patel, A. B. *et al.* The contribution of GABA to glutamate/glutamine cycling and energy metabolism in the rat cortex <em>in vivo</em&gt. *Proceedings of the National Academy of Sciences of the United States of America* **102**, 5588, doi:10.1073/pnas.0501703102 (2005).
84 Choi, I.-Y., Lee, S.-P., Kim, S.-G. & Gruetter, R. In Vivo Measurements of Brain Glucose Transport Using the Reversible Michaelis–Menten Model and Simultaneous Measurements of Cerebral Blood Flow Changes during Hypoglycemia. *Journal of Cerebral Blood Flow & Metabolism* **21**, 653-663, doi:10.1097/00004647-200106000-00003 (2001).
85 Michaelis, L., Menten, M. L., Johnson, K. A. & Goody, R. S. The original Michaelis constant: translation of the 1913 Michaelis-Menten paper. *Biochemistry* **50**, 8264-8269, doi:10.1021/bi201284u (2011).
86 Xin, L., Lanz, B., Lei, g. & Gruetter, R. Assessment of Metabolic Fluxes in the Mouse Brain in Vivo Using 1H-[13C] NMR Spectroscopy at 14.1 Tesla. *Journal of Cerebral Blood Flow & Metabolism* **35**, 759-765, doi:10.1038/jcbfm.2014.251 (2015).
87 de Graaf, R. A., Mason, G. F., Patel, A. B., Rothman, D. L. & Behar, K. L. Regional glucose metabolism and glutamatergic neurotransmission in rat brain <em>in vivo</em&gt. *Proceedings of the National Academy of Sciences of the United States of America* **101**, 12700, doi:10.1073/pnas.0405065101 (2004).
88 Henry, P.-G. *et al.* Decreased TCA cycle rate in the rat brain after acute 3-NP treatment measured by in vivo1H-{13C} NMR spectroscopy. *Journal of Neurochemistry* **82**, 857-866, doi:10.1046/j.1471-4159.2002.01006.x (2002).

89 Lizarbe, B. *et al.* Feasibility of in vivo measurement of glucose metabolism in the mouse hypothalamus by 1H-[13C] MRS at 14.1T. *Magnetic Resonance in Medicine* **80**, 874-884, doi:10.1002/mrm.27129 (2018).
90 Duarte, J. M. N., Lanz, B. & Gruetter, R. Compartmentalized Cerebral Metabolism of [1,6-(13)C]Glucose Determined by in vivo (13)C NMR Spectroscopy at 14.1 T. *Frontiers in neuroenergetics* **3**, 3-3, doi:10.3389/fnene.2011.00003 (2011).
91 de Graaf, R. A., Rothman, D. L. & Behar, K. L. State of the art direct 13C and indirect 1H-[13C] NMR spectroscopy in vivo. A practical guide. *NMR in Biomedicine* **24**, 958-972, doi:10.1002/nbm.1761 (2011).
92 Kumaragamage, C. *et al.* In vivo proton observed carbon edited (POCE) 13C magnetic resonance spectroscopy of the rat brain using a volumetric transmitter and receive-only surface coil on the proton channel. *Magnetic Resonance in Medicine* **79**, 628-635, doi:10.1002/mrm.26751 (2018).
93 Mueller, S. G. *et al.* Hippocampal atrophy patterns in mild cognitive impairment and Alzheimer's disease. *Human brain mapping* **31**, 1339-1347, doi:10.1002/hbm.20934 (2010).
94 Tepest, R. *et al.* Hippocampal Surface Analysis in Subjective Memory Impairment, Mild Cognitive Impairment and Alzheimer's Dementia. *Dementia and Geriatric Cognitive Disorders* **26**, 323-329, doi:10.1159/000161057 (2008).
95 Zhu, H. *et al.* Impairments of spatial memory in an Alzheimer's disease model via degeneration of hippocampal cholinergic synapses. *Nature Communications* **8**, 1676, doi:10.1038/s41467-017-01943-0 (2017).
96 Juchem, C. & de Graaf, R. A. B(0) magnetic field homogeneity and shimming for in vivo magnetic resonance spectroscopy. *Analytical biochemistry* **529**, 17-29, doi:10.1016/j.ab.2016.06.003 (2017).
97 Shaka, A. J., Keeler, J., Frenkiel, T. & Freeman, R. An improved sequence for broadband decoupling: WALTZ-16. *Journal of Magnetic Resonance (1969)* **52**, 335-338, doi:https://doi.org/10.1016/0022-2364(83)90207-X (1983).
98 Simpson, R., Devenyi, G. A., Jezzard, P., Hennessy, T. J. & Near, J. Advanced processing and simulation of MRS data using the FID appliance (FID-A)—An open source, MATLAB-based toolkit. *Magnetic Resonance in Medicine* **77**, 23-33, doi:10.1002/mrm.26091 (2017).
99 Dehghani M, M., Lanz, B., Duarte, J. M. N., Kunz, N. & Gruetter, R. Refined Analysis of Brain Energy Metabolism Using In Vivo Dynamic Enrichment of 13C Multiplets. *ASN neuro* **8**, 1759091416632342, doi:10.1177/1759091416632342 (2016).
100 Itoh, Y., Abe, T., Takaoka, R. & Tanahashi, N. Fluorometric determination of glucose utilization in neurons in vitro and in vivo. *J Cereb Blood Flow Metab* **24**, 993-1003, doi:10.1097/01.Wcb.0000127661.07591.De (2004).
101 Nehlig, A. & Coles, J. A. Cellular pathways of energy metabolism in the brain: Is glucose used by neurons or astrocytes? *Glia* **55**, 1238-1250, doi:10.1002/glia.20376 (2007).
102 Walter, A. *et al.* Glycerophosphocholine is elevated in cerebrospinal fluid of Alzheimer patients. *Neurobiology of Aging* **25**, 1299-1303, doi:https://doi.org/10.1016/j.neurobiolaging.2004.02.016 (2004).

103 Duarte, J. M. & Gruetter, R. Glutamatergic and GABAergic energy metabolism measured in the rat brain by (13) C NMR spectroscopy at 14.1 T. *J Neurochem* **126**, 579-590, doi:10.1111/jnc.12333 (2013).
104 Sibson, N. R. *et al.* In vivo (13)C NMR measurement of neurotransmitter glutamate cycling, anaplerosis and TCA cycle flux in rat brain during. *J Neurochem* **76**, 975-989, doi:10.1046/j.1471-4159.2001.00074.x (2001).
105 van Eijsden, P., Behar, K. L., Mason, G. F., Braun, K. P. & de Graaf, R. A. In vivo neurochemical profiling of rat brain by 1H-[13C] NMR spectroscopy: cerebral energetics and glutamatergic/GABAergic neurotransmission. *J Neurochem* **112**, 24-33, doi:10.1111/j.1471-4159.2009.06428.x (2010).
106 Voevodskaya, O. *et al.* Brain myoinositol as a potential marker of amyloid-related pathology. *Neurology* **92**, e395, doi:10.1212/WNL.0000000000006852 (2019).
107 Huang, W. *et al.* High brain myo-inositol levels in the predementia phase of Alzheimer's disease in adults with Down's syndrome: a 1H MRS study. *Am J Psychiatry* **156**, 1879-1886, doi:10.1176/ajp.156.12.1879 (1999).
108 Waragai, M., Moriya, M. & Nojo, T. Decreased N-Acetyl Aspartate/Myo-Inositol Ratio in the Posterior Cingulate Cortex Shown by Magnetic Resonance Spectroscopy May Be One of the Risk Markers of Preclinical Alzheimer's Disease: A 7-Year Follow-Up Study. *J Alzheimers Dis* **60**, 1411-1427, doi:10.3233/JAD-170450 (2017).
109 Voevodskaya, O. *et al.* Myo-inositol changes precede amyloid pathology and relate to APOE genotype in Alzheimer disease. *Neurology* **86**, 1754, doi:10.1212/WNL.0000000000002672 (2016).
110 Hammen, T. & Kuzniecky, R. in *Handbook of Clinical Neurology* Vol. 107 (eds Hermann Stefan & William H. Theodore) 399-408 (Elsevier, 2012).
111 Murray, M. E. *et al.* Early Alzheimer's disease neuropathology detected by proton MR spectroscopy. *The Journal of neuroscience : the official journal of the Society for Neuroscience* **34**, 16247-16255, doi:10.1523/JNEUROSCI.2027-14.2014 (2014).
112 Schott, J. M. *et al.* Short echo time proton magnetic resonance spectroscopy in Alzheimer's disease: a longitudinal multiple time point study. *Brain* **133**, 3315-3322, doi:10.1093/brain/awq208 (2010).
113 Marjanska, M., McCarten, J. R., Hodges, J. S., Hemmy, L. S. & Terpstra, M. Distinctive Neurochemistry in Alzheimer's Disease via 7 T In Vivo Magnetic Resonance Spectroscopy. *J Alzheimers Dis* **68**, 559-569, doi:10.3233/jad-180861 (2019).
114 Demougeot, C. *et al.* N-Acetylaspartate, a marker of both cellular dysfunction and neuronal loss: its relevance to studies of acute brain injury. *Journal of Neurochemistry* **77**, 408-415, doi:10.1046/j.1471-4159.2001.00285.x (2001).
115 Antuono, P. G., Jones, J. L., Wang, Y. & Li, S. J. Decreased glutamate + glutamine in Alzheimer's disease detected in vivo with (1)H-MRS at 0.5 T. *Neurology* **56**, 737-742, doi:10.1212/wnl.56.6.737 (2001).
116 Fayed, N., Modrego, P. J., Rojas-Salinas, G. & Aguilar, K. Brain glutamate levels are decreased in Alzheimer's disease: a magnetic resonance spectroscopy study. *Am J Alzheimers Dis Other Demen* **26**, 450-456, doi:10.1177/1533317511421780 (2011).
117 Revett, T. J., Baker, G. B., Jhamandas, J. & Kar, S. Glutamate system, amyloid ß peptides and tau protein: functional interrelationships and relevance to Alzheimer disease

pathology. *Journal of psychiatry & neuroscience : JPN* **38**, 6-23, doi:10.1503/jpn.110190 (2013).

118 Campos-Pea, V. & Antonio, M. (2014).

119 Kulijewicz-Nawrot, M., Syková, E., Chvátal, A., Verkhratsky, A. & Rodríguez, J. J. Astrocytes and glutamate homoeostasis in Alzheimer's disease: a decrease in glutamine synthetase, but not in glutamate transporter-1, in the prefrontal cortex. *ASN neuro* **5**, 273-282, doi:10.1042/AN20130017 (2013).

120 O'Donovan, S. M., Sullivan, C. R. & McCullumsmith, R. E. The role of glutamate transporters in the pathophysiology of neuropsychiatric disorders. *npj Schizophrenia* **3**, 32, doi:10.1038/s41537-017-0037-1 (2017).

121 Matos, M., Augusto, E., Oliveira, C. R. & Agostinho, P. Amyloid-beta peptide decreases glutamate uptake in cultured astrocytes: involvement of oxidative stress and mitogen-activated protein kinase cascades. *Neuroscience* **156**, 898-910, doi:10.1016/j.neuroscience.2008.08.022 (2008).

122 Bathina, S. & Das, U. N. Brain-derived neurotrophic factor and its clinical implications. *Archives of medical science : AMS* **11**, 1164-1178, doi:10.5114/aoms.2015.56342 (2015).

123 Chen, S. *et al.* CaMKII is involved in cadmium activation of MAPK and mTOR pathways leading to neuronal cell death. *J Neurochem* **119**, 1108-1118, doi:10.1111/j.1471-4159.2011.07493.x (2011).

124 Gauthier, S., Herrmann, N., Ferreri, F. & Agbokou, C. Use of memantine to treat Alzheimer's disease. *CMAJ : Canadian Medical Association journal = journal de l'Association medicale canadienne* **175**, 501-502, doi:10.1503/cmaj.1060168 (2006).

125 Reisberg, B. *et al.* Memantine in Moderate-to-Severe Alzheimer's Disease. *New England Journal of Medicine* **348**, 1333-1341, doi:10.1056/NEJMoa013128 (2003).

126 Group, A. R. *et al.* Cognitive function over time in the Alzheimer's Disease Anti-inflammatory Prevention Trial (ADAPT): results of a randomized, controlled trial of naproxen and celecoxib. *Archives of neurology* **65**, 896-905, doi:10.1001/archneur.2008.65.7.nct70006 (2008).

127 Hershey, L. A. & Lipton, R. B. Naproxen for presymptomatic Alzheimer disease. *Neurology* **92**, 829, doi:10.1212/WNL.0000000000007233 (2019).

128 Gasparini, L., Ongini, E. & Wenk, G. Non-steroidal anti-inflammatory drugs (NSAIDs) in Alzheimer's disease: old and new mechanisms of action. *Journal of Neurochemistry* **91**, 521-536, doi:10.1111/j.1471-4159.2004.02743.x (2004).